DESIGN AND ENGINEERING OF 3D COLLAGEN-FIBRONECTIN SCAFFOLDS FOR WOUND HEALING AND CANCER RESEARCH

By

Maryam Asadishekari

Thesis submitted to the Faculty of Graduate and Postdoctoral Studies

in partial fulfillment of the requirements for

Master of Applied Science

in

Biomedical Engineering

FACULTY OF ENGINEERING

UNIVERSITY OF OTTAWA

Abstract

Despite our understanding of the importance of the 3D environment on the behaviour of virtually every cell, most studies are still performed within 2D engineered cell culture devices. In this project, the main goal was to design and engineer tunable three-dimensional (3D) extracellular matrix (ECM)-mimicking scaffolds made of collagen and fibronectin (namely the two major building blocks of the ECM) that recapitulate the ECM structural and mechanical properties essential for wound healing and cancer research. Two different methods were implemented to fabricate 3D scaffolds.

First, 3D collagen scaffolds with a 'porous' structure (fabricated by a previous student via an ice-templating technique) were used. It was shown that, by increasing collagen concentration to 1.25 wt.%, homogenous scaffolds with interconnected pores (needed for cell invasion through the entire scaffold) were obtained. Fibronectin (Fn) was then incorporated using thermal and mechanical gradients to modify protein content and tune scaffolds microarchitecture. The effect of Fn coating of the collagen underlying structure on cell behaviour such as cell adhesion, invasion and matrix deposition was studied. Results showed that overall more cells adhered to Fn-coated scaffolds with respect to pure collagen scaffolds. Furthermore, our findings indicated that cells were also able to sense the conformation of the Fn coating (as assessed by Fluorescence Resonance Energy Transfer, FRET) since they deposited a more compact ECM on compact Fn coating while a more unfolded and stretched ECM was deposited on unfolded Fn coating.

Second, 3D more complex physiologically relevant scaffolds with a 'fibrillar' structure were fabricated via a cold/warm casting technique. Pure collagen scaffolds were first generated: in cold-cast scaffolds, clear thin and long collagen fibers were observed while warm-cast scaffolds were denser and comprised shorter collagen fibers. The effect of both collagen concentration and casting temperature on scaffolds' microstructure was studied. Our results indicate a preponderant effect of temperature. We further engineered dual-protein fibronectin-collagen fibrillar scaffolds by incorporating Fn fibers using thermal gradient. Clear Fn fibers were observed in some conditions. FRET assessment of Fn fibers also showed significant difference of Fn conformation. In this more advanced casting technique, cells were initially embedded into the scaffolds, which provided a more homogeneous cell distribution and a better tissue-mimicking setting. In each case, the effect of resulting ECM properties was tested via cell viability assays. Our data indicate that cells were

viable after 72 hours, they could proliferate inside the scaffolds and were able to spread in some conditions.

Collectively, our 3D ECM-mimicking scaffolds represent a new tunable platform for biological and biomaterial research with many potential applications in tissue engineering and regenerative medicine. Investigating cell behaviour in 3D ECM-mimicking environment will provide valuable insights to understand cancer progression and approaches to limit the progression and ultimately prevent metastasis.

Table of Contents

List of Figures

Acknowledgement

First and foremost, my most sincere gratitude goes to Dr. Delphine Gourdon for giving me the opportunity to work in her lab and providing invaluable guidance throughout my research program. Her patience, vision and encouragement have deeply inspired me. It was a great privilege and honor to work and study under her supervision.

My special thanks to Dr. Elie Ngandu Mpoyi for his help and valuable advice during my experiments and preparation of my thesis. He taught me that life is fantastic and no matter how hard, there is a way to enjoy every moment of it.

I would like to thank Ryan Hickey from Dr. Pellings' lab for generously devoting his time for training me when I joined the lab.

Also, many thanks to Mr. Andrew Ochalski, the manager of Cellular Imaging and Cytometry Facility who kindly trained me on Ziess confocal microscope and for his always being there to answer my questions.

I would also like to thank and acknowledge the following past and present members of the Gourdon lab for their contributions: Junhui Ye, Yifan Li, Kate Lerigoleur, Zian Shahid, Simardeep Dhindsa, Halimo Aden, Mihir Samak, Parisa Sadeghi and Naveena Janakiraman.

I dedicated this thesis to my lovely parents, Mohammadreza Asadishekari and Sedigheh Armanian who have always been there in my hardest of times, supported me, and loved me unconditionally. It is their love and prayers that have given the strength and courage to reach this point in my life. This is also for Ali Asadishekari, my wonderful brother, and my beautiful sister-in-law, Nazgol Shirazi. Being away from them, has been the most difficult task of my life.

This work was supported financially by a Natural Sciences and Engineering Research Council of Canada (NSERC) Discovery Grant under award RGPIN-2017-06784 (to Delphine Gourdon).

List of Abbreviations

2D	Two dimensional
3D	Three dimensional
AFM	Atomic force microscopy
ANOVA	Analysis of variance
DAPI	Diamidino-2-phenylindole dye
DMEM	Dulbecco's modified eagle medium
ECM	Extracellular matrix
ELISA	Enzyme-linked immunosorbent assay
FBS	Fetal bovine serum
Fn	Fibronectin
FRET	Forster resonance energy transfer
GdnHCl	Guanidine hydrochloride
PBS	Phosphate buffered saline
SEM	Scanning electron microscopy
VEGF	Vascular endothelial growth factor
TGF	Transforming growth factor
FGF	Fibroblast growth factor

Chapter 1: Introduction

Cells sense and respond to their microenvironment via trans-membrane proteins, thus regulate several physiological processes such as differentiation, gene expression, migration, morphology, angiogenesis and proliferation, as well as the response to drugs[1,2,3,4]. In vivo, cells reside within a complex three-dimensional (3D) structure – the extracellular matrix (ECM) – that provides mechanical and biochemical support while directing cellular behaviour[5]. To understand the concept of several complicated biological functions such as wound healing and cancer progression, it is essential to study ECM composition, structure and mechanics. This chapter presents ECM components, basic principles of wound healing process and cancer progression as well as the use of biomaterials to mimic complex ECM structures.

1.1 Extracellular Matrix

The ECM has been known as a 3D structure which supports cell adhesion[6] and signalling[4]. ECM is an essential non-cellular structural component of cellular organisms. It is a complex network of several macromolecules including proteins, proteoglycans and glycoproteins with specific physical and biochemical properties[7]. It is mostly made up of water, proteins and polysaccharides but chemical composition of ECM is different depending on the tissue functions and the cells that deposited them. For example, collagen I is abundant in tendons while collagen IV is ubiquitous in basement membranes[8]. ECM has different characteristics in terms of chemical and mechanical properties. Structural, biochemical and biomechanical properties of the ECM should be taken into account as they can disturb cell activities[9]. The structure of the ECM plays an important role as it influences cell behaviour including cell attachment, migration and proliferation[10]. While mechanical properties are responsible for specific cell activities including cell differentiation, apoptosis and tissue function, they control cell signalling through which cells sense and respond to their environment. Structural and mechanical properties of the ECM are related. A structural or morphological change in the ECM scaffold characteristic would also affect its biomechanical feature, hence also impact cells behaviour. In tumour tissues, remodelled and abnormally deposited collagens I, III and IV promote increased stiffness[11,12]. While healthy tissues contain more relaxed

proteins such as collagen type I and III, elastin and Fn[13]. Changes in ECM could cause genetic disorders and well-known human diseases such as bone[14] and cardiovascular disease[15].

In terms of dimensionality of the ECM, cells in tissues and organs reside in (and adhere to) 3D fibrillar ECM while in basement membrane cells attach to 2D surfaces[16]. It should be noted that the relationship between cells and the ECM is mutual. Cells interact with the ECM to rearrange and deposit ECM constituents, while alterations in the ECM affect neighbouring cells and change their behaviour[9].

The ECM is constituted of two structural groups: interstitial (stroma) and basement. In interstitial ECM, matrix assembly is fibrillar around cells while basement ECM is less porous and more compact with sheet-like structure[17,18,19]. Basement membrane mainly contains laminins and collagen IV[20]. Due to significant roles of the ECM, study of its structures and components helps to better understand cell behaviour and functions. The key components of the ECM are collagen, fibronectin, elastins and laminins, and for this study only the first two components are discussed below.

1.1.1 Collagen

Collagen is one of the most abundant proteins in tissues and the ECM. Almost 30% of the dry weight of mammalians consists of collagen[21,5]. Most portions of connective tissues, skins, muscles, tendons and bones consist of collagen fibrils. Collagen fibers take up of almost 90% of bone proteins[22]. Collagen networks act as scaffolds in most hard and compliant tissues including bone, tendon, blood vessels and skin. It provides toughness in bones. Therefore, changes in collagen structure when ageing causes osteoporotic fractures[23].

29 different types of collagen are identified among which some of them form fibrils including type I, II and III[24,25]. Collagen is characterised by the presence of a triple helical repeat. The triple helix contains three α chains in which several amino acids are placed together. The structure of each amino acid follows -Gly-X-Y- sequence. Glycine is crucial in the sequence to establish structured triple helixes[26]. Triple helical units form collagen fibrils. Further collagen fibers are formed by cross-linked fibrils[27].

One of the most novel biomaterials currently use in cosmetic and drug delivery fields is collagen, particularly type I. Collagen I is considered the gold standard in tissue engineering and regenerative medicine. It is mostly engineered in the fibrillar form or sponges and sheets. Apart from natural polymers, synthetic biomaterials are widely used due to their easy fabrication and abundance[28]. Collagen I is widely used due to its biodegradability and biocompatibility. Since collagen is a natural protein, cells would consider it as a native component due to being immunologically safe. So, it is applicable in several tissue engineering fields such as implants[29].

In terms of biodegradability, degradability of collagen in biomaterials promotes tissue reconstruction[30]. Collagen degrades by matrix metalloproteinases (MMPs) as a part of collagenase that are in charge of breaking the peptide bonds in collagens[31]. After breaking bonds, enzymes would degrade the collagen molecules[32].

Collagen-based biomaterials have been categorized into two groups. Either they are decellularized ECM, mostly contains collagen or they are derived from collagen-based tissues[21]. Collagen I can be derived from most living animals. However, generally used sources are bovine tendon and skin, rat tail and porcine skin. Bovine-derived collagen I mostly is used as skin substitutes to promote wound healing process. One of the most popular collagen-based applications is wound dressings to cover the injuries and promote ulcer treatment. The common commercial skin replacements are Integra™, Alloderm™ and Amniograpg™ [33].

1.1.2 Fibronectin

Fibronectin (Fn) is one of the most crucial proteins along with collagen in the ECM. It is a large multidomain protein with two subunits of almost the same molecular weight ranging from 230 to 270 kDa, as determined by the difference splice isoforms of the mRNA, and linked by C-terminal disulfide bonds (COOH) and N-terminal[34]. The most crucial three modules are Fn I, Fn II and Fn III. Fn I and II are mechanically stable due disulfide bonds while Fn III lack these disulphide bonds, which makes them sensitive to external mechanical forces[35]. Figure 1.1 shows that there are twelve type I modules on Fn with fifteen type III modules and only two modules of type II. One of the main binding sites on Fn is III_1 (anastellin) that promotes aggregation of Fn into fibrils. Due to several binding sites on Fn, it can interact and bind to cells and molecules at the same time[18].

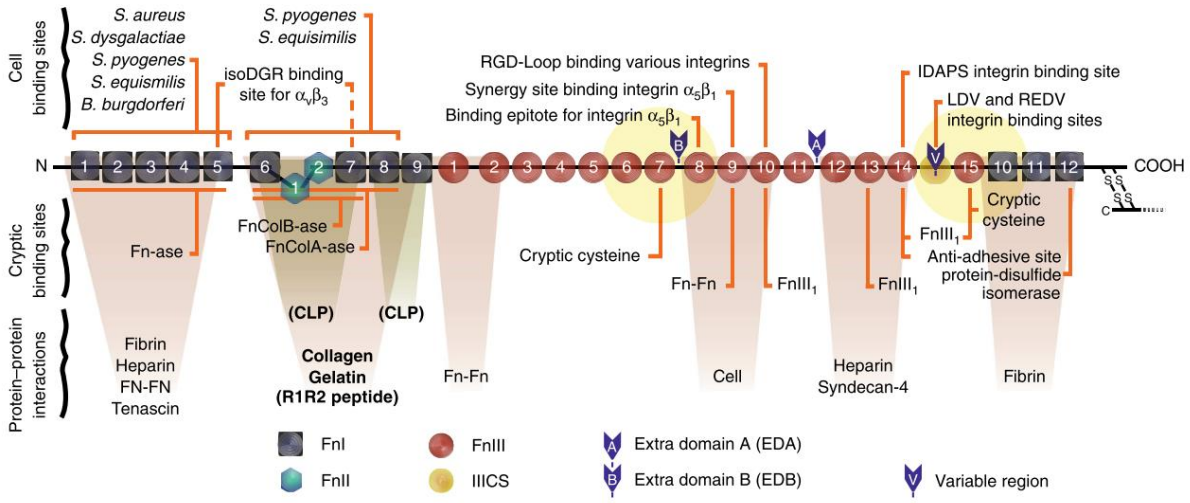

Figure 1.1 **Schematic of Fn molecule showing type I, II and III modules with Fn's binding sites**. Adapted from (Mechanical forces regulate the interactions of fibronectin and collagen I in extracellular matrix. Kubow et al. 2015. DIO: 10.1038/ncomms9026).

Fn has multiple recognition sites for cells, including the well characterized RGD loop (Arg-Gly-Asp) and for other ECM proteins including collagen ($I_{6\text{-}9}$ and $II_{1,2}$) and fibrin (Fibrin I and Fibrin II)[36]. A major recognition site for cells on Fn, the RGD loop, resides on Fn III_{10}[35]. Having various recognition sites, Fn conformation could be observed by labelling the desired site[36].

Fn I contains 45 amino acids. Fn I consists of a double-stranded anti-parallel β sheet and a triple-stranded anti-parallel β sheet knit together. Fn II contains approximately 40 amino acids. It consists of two perpendicular anti-parallel β sheets[37]. Module I and II conformation is unlikely to change due to disulfide bonds that stabilize them. Fn III is the most crucial modulus since it contains two major recognition sites for cells, RGD loop resides on III_{10} and the synergy site located on the adjacent Fn III_9. RGD loop is involved in most cell-binding interactions. While some integrins such as $\alpha v\beta_3$ require only RGD loop to bind to the Fn[38], some integrins such as $\alpha_5\beta_1$ need an additional binding site, pro-his-ser-arg-asp (PHSRN) synergy site[39]. Fn conformation occurs on this modulus due to the lack of disulfide bonds. Seven β strands make four anti-parallel β sheets to form Fn III modules[40].

Fn is found in two forms of soluble (plasma Fn) that circulate in the blood and insoluble Fn (cellular Fn), which is cell-deposited Fn. Once injured, plasma Fn plays a role at early stages of wound healing and hemostasis. Cellular Fn has a role in late stages of wound healing and fibrosis as well as angiogenises[41,42]. Fn plays an important role in different applications. In skin, it enhances cell-tissue interactions. In wound healing process, it helps restoring tissue structures and in vitro Fn promotes cell adhesion through protein-based surfaces[42].

The conformation of Fn is of great importance as any change is likely to affect the binding sites and cell signalling. It is currently arguable whether Fn conformation (near to compact or unfolded) changes outside or inside cell signalling. Fn is considered compact when Fn arms are crossed-over while it is unfolded when the dimeric arms are separated[36] (Figure 1.2). Changes in Fn conformation may also result in activation and release of specific enzymes such as matrix metalloproteinase-2 (MMP-2) that supports tumour invasion and metastasis. Stiffness of the ECM should be considered as well as conformation, since invasive cells favour stiffer ECM to metastasize[35].

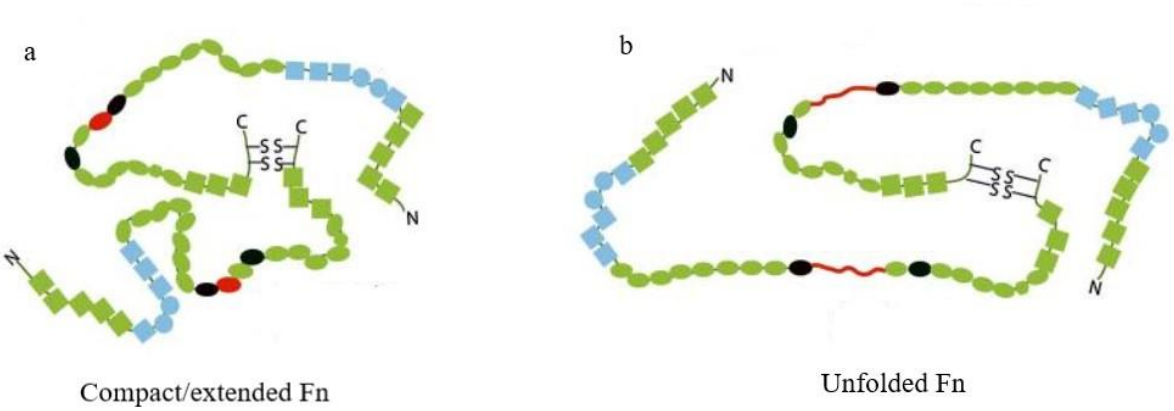

Figure 1.2 **Schematic of Fn conformation.** (a) Compact/extended Fn in the healthy microenvironment. (b) Unfolded Fn in the tumour microenvironment. Adapted from (Fibronectin mechanobiology regulates tumorigenesis. Wang et al. 2016. DIO: 10.1007/s12195-015-0417-4).

It is established that the presence of Fn in cell environment is necessary for deposition and assembly of collagen fibers. Besides, Fn is found to be the first ECM protein deposited by isolated cells[43]. The existence of two distinct Fn fibers populations in a 3D ECM model was proven, relaxed Fn fibers adsorbed to collagen and unfolded Fn fibers with no colocalization with collagen fibers[44].

1.2 Fluorescence Resonance Energy Transfer

Fluorescence resonance energy transfer (FRET) has been used to measure the distance between proteins (intermolecular) or the distance between amino acids within a protein (intramolecular). FRET is a distance-related, non-radiative transfer of energy between donor and acceptor fluorophores. Referring to the Jablonski energy level diagram (Figure 1.3), an excited donor fluorophore can go back to steady state energy level either by losing its energy through fluorescence emission or instead by transferring the energy to the acceptor fluorophore under two circumstances: the acceptor molecule should be in close proximity to the donor molecule (1-10nm) and the absorption spectrum of the acceptor should overlap with the emission spectrum of the donor[45] (Figure 1.4).

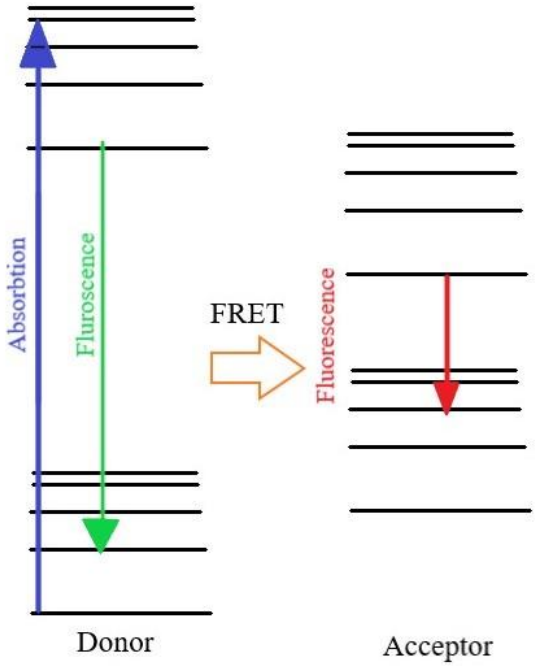

Figure 1.3 **Jablonski energy level diagram**. August 8 2018, retrieved from https://commons.wikimedia.org.

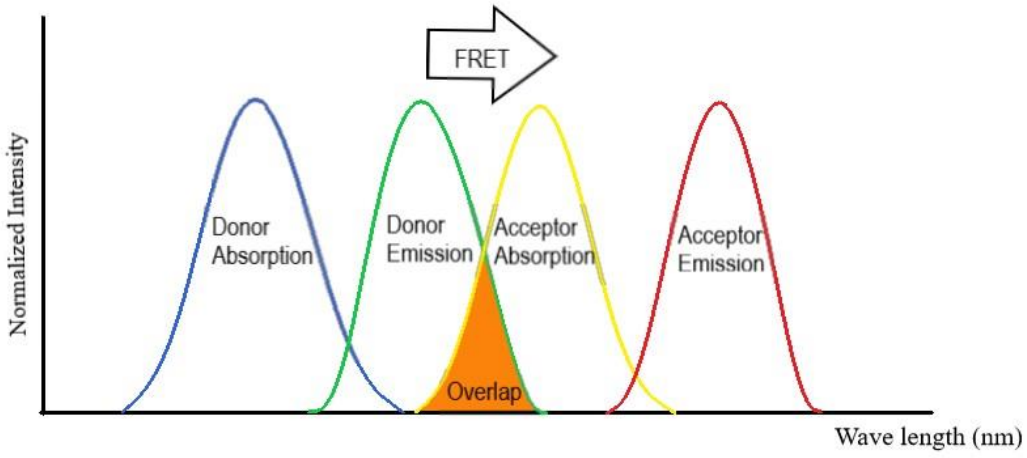

Figure 1.4 **Absorption and emission of donor and acceptor molecules spectrum**. Adapted from (A quantitative protocol for dynamic measurements of protein interactions by Förster resonance energy transfer-sensitized fluorescence emission. Elder et al. 2009. DIO: 10.1098/rsif.2008.0381.focus).

The efficiency of the FRET energy transfer (E) is very sensitive to distance between donors and acceptors (inversely to the sixth power of the distance): $E = R_o^6 / (R_o^6 + r^6)$, Where R_o called Forster radius, is the distance where half of the energy is transferred and r is the distance between donor and acceptor. FRET is calculated as the ratio of average fluorescence signal emitted by acceptor fluorophores over average fluorescence signal emitted by donor fluorophores when donors are directly excited by an appropriate laser line[46].

FRET Ratio = I_A/I_D

A pair of donor and acceptor fluorophores would be needed to visualize the distance between/within proteins. CFP (cyan fluorescent protein)-YFP (yellow fluorescent protein), GFP (green fluorescent protein)-RFP (red fluorescent protein), Alexa488-Cy3 and Alexa488-Alexa 546 have been frequently used as donor-acceptor pairs[47]. By tuning concentration of donor and acceptor (usually higher concentration of acceptors to donors) and considering the overlap spectrum of donor and acceptor (larger overlap area), higher FRET efficiency could be obtained[48].

Fluorescence microscopy has improved FRET technology since images could be analyzed quantitatively. Protein-protein interactions have become visualized with the aid of FRET microscopy[49]. FRET imaging has always been a concern due to photobleaching, autofluorescence,

detector and background signals. Confocal microscopy with the aid of custom mathematical codes and deconvolution, has resolved some issues including deducting background noise[50].

1.2.1 FRET Labeled Fibronectin

Intramolecular FRET can be exploited to measure the various conformations fibronectin can adopt in vitro and FRET-labeled Fn has been used as a mechanical strain sensor[51]. Since Fn is a large molecule with several binding sites, desired sites could be labeled (Figure 1.5). The average distance between fluorophores would be measured and reported in FRET ratio.

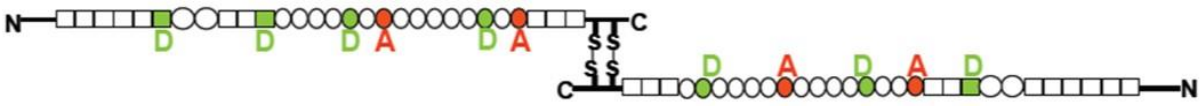

Figure 1.5 **Schematic of Fn labeling**. Adapted from (Force-induced unfolding in the extracellular matrix of living cells. Smith M et al. 2007. DIO: 10.1371/journal.pbio.0050268).

FRET Fn is sensitive to changes in conformation of type III modules. Fn conformation varies in solutions with different pH level. FRET calibration is performed in different concentration of denaturant guanidine hydrochloride (GdnHCL). Fn in solutions is folded with crossed arms while in moderate denaturing solutions, (>1 M GdnHCL), intramolecular protein connection is lost between two arms and Fn starts unfolding. In sever denaturing solutions (<1 M GdnHCL), Fn loses secondary structure and Fn III modules starts unfolding which results in reduction in FRET ratio (Figure 1.6). To summarize, in solutions with <1 M GdnHCL concentration, Fn starts to lose secondary structure and in 4M is totally denatured[52,53].

Figure 1.6 **Schematic of Fn structure in solution**. (a) Compact (b) extended (c) unfolded. Adapted from (Protein-crystal interface mediates cell adhesion and proangiogenic secretion. Wu et al. 2017. DIO: 10.1016/j.biomaterials.2016.11.043).

Although FRET has been introduced many years ago, it has only been recently used in biological studies[54] particularly intramolecular FRET, which allows one to determine distances between labeled residues within a single molecule (intramolecular distance), hence directly linked with molecular conformation[55,56]. One of the most frequent applications of FRET is in molecular biology such as biotechnology, medicine and biophysics to study molecular scale interactions[57,58] since it is sensitive to distances in the range of 10-100 A°, which covers membranes and molecules size[59,60,61]. FRET technique has been used in biological systems to detect changes in single molecule conformations[62,63,64]. The study of Fn conformations has attracted many scientists due to its crucial role in biological fields and tissue engineering such as wound healing and cancer studies[65,66].

Smith et al studied the effect of cell-generated forces on Fn fibers unfolding. FRET confocal images were analyzed quantitatively using customized color-coded Matlab code. Blue pixels demonstrated unfolded Fn (Figure 1.7). Their results indicated the coexistence of stretched and unfolded Fn fibers (due to cell generated forces unfolding of some Fn III modules) with more relaxed and compact Fn fibers in the physiological ECM[36].

It is proven that cells sense their environment and respond by changing their behaviour including matrix deposition and remodelling. Cell-derived matrix has a key role in overall ECM rigidity and cell differentiation[67].

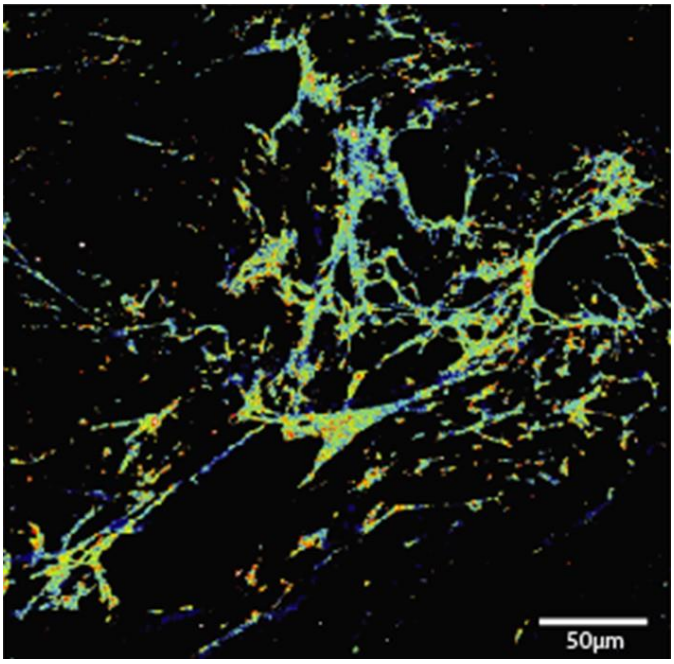

Figure 1.7 **Cell-deposited Fn fibers in 24-hour living cell culture**. Adapted from (Force-Induced Unfolding of Fibronectin in the Extracellular Matrix of Living Cells. Smith M et al. 2007. DIO: 10.1371/journal.pbio.0050268).

FRET imaging has helped scientists to study cell-deposited matrix conformation. To address the issue of ECM and substrate stiffness, Fn conformation was studied on rigid and flexible polyacrylamide surfaces using FRET. It was shown that Fn-deposited fibers on rigid surfaces were noticeably more unfolded than on flexible surfaces. Furthermore, it was suggested that cell-made Fn fibers became more stretched and lost their secondary structure over time[52].

1.3 Biomaterials

Biomaterials have been described as any material in any form such as solid, liquid, gels that interact with biological systems to serve their ultimate goal of reconstructing or replacing tissues[68]. The history of using biomaterials dates back to 3000 BC where Egyptians used linen as sutures and Mayas used mother of pearl as tooth implants. Biomaterials became more effective when biocompatibility was a key component of biomaterials research. Metals were the first biomaterials utilized as metal wires to stabilize bone fractures. Then they appeared in several (mostly

orthopaedic) applications as bone screws, hip and knee prosthesis, etc. The improvement of biomaterials, specifically metals, advanced significantly during word war II[69].

Biomaterials have been categorized under three groups of synthetic, natural and hybrid biomaterials. Metals, polymers, ceramics and composites are considered as synthetic biomaterials. Metals have been used in dental and orthopaedic implants due to their strength and toughness. Commonly used metals are stainless steel, titanium and cobalt alloys. Polymers are also commonly used in medical fields due to their diversity in compositions and properties. Polyvinylchloride (PVC), polyethylene (PE) and polymethylmethacrylate (PMMA) are the most frequent polymers used in medical fields. Finally, ceramics are used as implants and/or coatings because they are inert materials and highly resistant to wear. Zirconia and alumina are used as coating and orthopaedic implants. Composites are combination of biomaterials that are designed for specific applications. They can be combined together and offer new properties for specific applications such as biosensors and microelectrodes[70]. Due to low biocompatibility and lack of tissue interaction of synthetic biomaterials, natural biomaterials such as collagen, chitosan, fibrin and alginate have been widely used. Their chemical composition is similar to biological tissues and they can interact with the host. Natural biomaterials are usually built up of proteins, polysaccharides and polynucleotides. The source of natural biomaterials are plants, animals or humans[68].

Biomaterials are available in a wide variety of selections. Several features such as clinical application, cost and engineering process should be taken into consideration upon choosing biomaterials. Application of biomaterials has been developed in medicine from implants and restoring tissues to drug delivery and gene therapies[68].

Tissue engineering is an emerging field with the purpose of providing structures for injured organs and tissues[71]. Biomaterials are widely used in tissue engineering field since they could be fabricated in three dimensional (3D) to support cells and control cell behavior[72]. The ultimate goal of biomaterial scaffolds is to provide ECM-mimicking platforms to control cell behaviour including proliferation, migration and death by cell-matrix interactions. To achieve this goal, scaffolds need to support cell invasion and communications by high porosity, large pore sizes and interconnected pores[73]. They are also made with ECM proteins for example fibronectin, laminin and collagen IV to better mimic the ECM and improve cell attachment properties[74].

Hydrogels have attracted attentions in many biomedical applications such as tissue engineering and drug delivery because of their aqueous nature, their biodegradability and their biocompatibility. Hydrogels gelatinize when hydrophilic polymer chains are cross-linked. Several methods of physical crosslinking such as thermo condensation, self-assembly, ionic, electrostatic and chemical crosslinking are available for hydrogels[75]. They can be formed by thermal gelation due to change in temperature which results in packed polymer backbones and changed hydrogel solubility[76].

Apart from biomaterials that provide ECM-mimicking scaffolds for cells, decellularized tissues as scaffolds have attracted attentions since they contain natural proteins and cell-made matrix. They have been used in cardiac reconstructions[77], cartilage sheets[78] and orthopaedic scaffolds[79].

However, there is no control over the composition and structure of decellularized tissues such as density and shape. Moreover, a donor tissue needs to be available which results in greater use of natural/synthetic biomaterials[80].

Biomaterials have been fabricated through several techniques to provide an environment with desired physical and chemical properties for cells depending on the applications. They can be engineered to porous and fibrillar structures. Most common techniques are electrospinning, freeze-drying and self-assembly. Electrospinning is a technique to produce nanofibers networks. In electrospinning, a solution is ejected on a collector through a needle while high voltage is applied and the solvent evaporates resulting in a solid network. Electrospinning is a cost-effective method to fabricate nanofibers, however, it is not adapted to engineer complex and heterogeneous structures, as there is no control over pore structure and fiber homogeneity[81]. In freeze-casting technique, a colloidal/polymeric solution is frozen at -80 °C then placed in a chamber with reduced pressure. The ice crystals formed are then sublimated, which results in porous scaffolds[82]. The main advantage of freeze-casting is control of pore structure and size by tuning the freezing rate and pH[83]. In self-assembly, molecules form structures by non-covalent bonding such as hydrogen bonds and van der Waals forces. The most common protein fabricated through self-assembly is collagen where triple helical units turn into collagen fibers. Fiber structure can be tuned by varying the pH[84].

1.3.1 Applications

Most scientists in tissue engineering fields are trying to engineer platforms to best mimic the ECM. They combine different biomaterials with cells using several methods of fabrication. Collagen as a natural protein has been widely used in biomedical fields[85]. It can be assembled into fibrillar, sheets and sponges substrates. One of the most predominant applications of collagen in a solid form is in ophthalmology. Collagen has been used as a corneal substitute, sutures and lenses. Liquid collagen gels have also been recently used as injectable biomaterials in skin wound healing dressings[86]. Dense collagen scaffolds have been engineered demonstrating same collagen density as in tissues, which is roughly around 10 wt.%. These scaffolds have been shown to promote proliferation, viability and migration[80].

Earlier in the Gourdon group, interconnected porous collagen scaffolds were fabricated by Yifan Li (a former master student) using a previously published freeze-casting technique[87]. Networks with varied porosity were achieved by changing the concentration of collagen. The overall effect of collagen concentration on several scaffolds materials properties was investigated. Figure 1.8 displays scanning electron microscopy (SEM) images of collagen porous scaffolds generated with varied collagen concentration showing that collagen concentration could be used to control the size of pores in the network, under constant freezing temperature (-10°C). By increasing collagen concentration from 0.5 wt.% to 1.25 wt.%, pores' diameter decreased from ~ 214 µm (with pore area of ~ 0.676 m^2/g) to ~ 35 µ (with pore area of ~ 2.013 m^2/g).

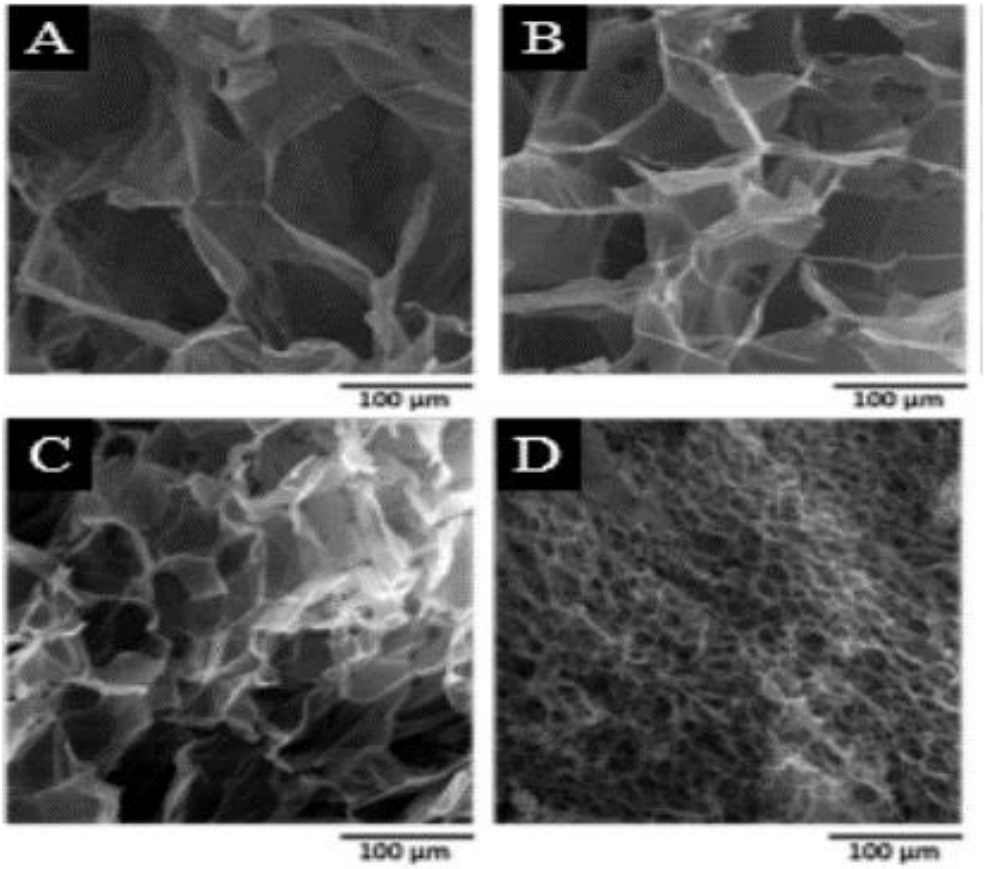

Figure 1.8 **SEM images of porous collagen scaffolds** with (A) 0.5 wt.%, (B) 0.75 wt.%, (C) 1.0 wt.% and (D) 1.25 wt.% collagen concentration fabricated by ice-templating technique at -10°C. Images are courtesy from Li, Yifan; Ye, Junhui, former lab students.

Additionally, dynamic mechanical analyzer (DMA Q800; TA Instrument) was used to measure the mechanical properties of collagen scaffolds. Figure 1.9 shows compressive modulus of collagen scaffolds with different concentrations. It was observed that compressive modulus of the scaffolds increased with increasing collagen concentration with the highest stiffness (1720 ± 300 Pa) achieved for the 1.25 wt.% collagen scaffolds.

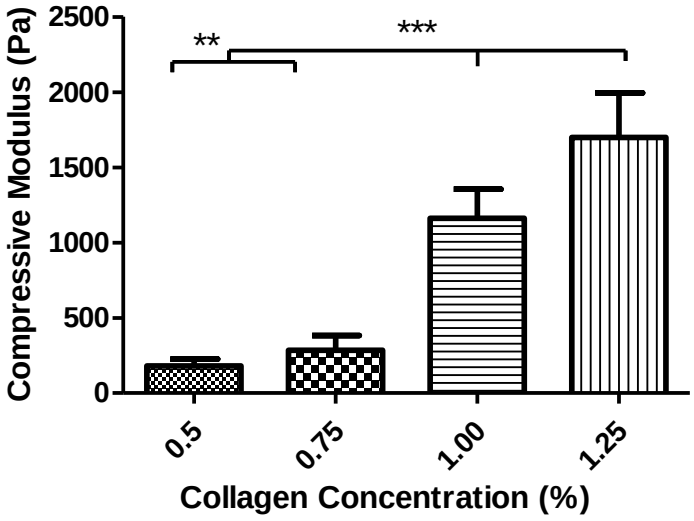

Figure 1.9 **Compressive modulus of scaffolds** with 0.50, 0.75, 1.00 and 1.25 wt.% collagen concentration. Compressive modulus was measured by the DMA. The compressive modulus increased by increasing the collagen concentration. Images are courtesy from Li, Yifan; Ye, Junhui, former lab students. (**P<0.001, ***P<0.0001) Mean ± SD.

Most engineered 3D hydrogel-based platforms lack a fibrillar structure. Fibrillar scaffolds best mimic the ECM since focal adhesions form only in fibrillar settings. It is suggested that fibrillar structures improve focal adhesion formation, cells interactions with their substrates through integrins, and local collagen matrix remodelling[88]. To study cell behaviour and signalling, the ability to control ECM locally is useful in case of angiogenesis and metastasis. During metastasis it is shown that cells alter the alignment and density of collagen fibers locally. The formation of fibers is dependent on different parameters such as concentration, pH and temperature in bulk collagen gels[89]. Alterations in vascularization due to ECM changes indicate breast cancer development. It has been shown that stiffer substrates enhanced collagen fibers alignment[90] suggesting that alignment impacts vascularization[91].

Biomaterials have been used in cancer research to study cell behaviour along with the ECM properties during tissue morphogenesis. Biomaterials could be engineered into platforms that mimic either healthy tissue or tumour microenvironmental properties. Comparing cell behaviour leads to understanding cancer functions. Staunton and coworkers designed two collagen scaffolds by controlling temperature and collagen concentration that mimic tumour (stiffer) and healthy

(more compliant) environment. Their findings indicate much greater storage modulus (three-fold) for scaffolds placed at low temperature (4°C) compared to high tempertaure (37°C)[92].

1.4 Wound Healing

Acute non-healing injuries develop as a result of illness (e.g., diabetes). There are usually three different approaches to wound healing such as autografts, allografts and biocompatible wound dressings. Recently, novel approaches involving soft tissue scaffolds that mimic the ECM have also been used to replace tissues and accelerate wound healing process[17]. Skin wound healing process consists of several complex phases. Once injured, four main phases of hemostasis, inflammatory reaction, cell proliferation and remodelling of tissue occur to heal the wound.

The early reaction toward injuries is hemostasis, which is formation of clot to stop bleeding. As soon as being injured, growth factors and several cell types are recruited to the wound site[93]. The blood at the site of damage interacts with ECM components mostly collagen and promote platelets to secrete clotting factors including fibrin, fibronectin and vitronectin to form a clot[94]. It is then followed by inflammatory stage in which inflammatory cells are called at the site to reactive oxygen species and clean up the site from dead cells. It prepares the site for next stage of the proliferative phase[95]. Fibroblasts proliferate during this phase and deposit high amounts of extracellular matrix such as collagen and fibronectin which both play a key role during this stage. The excess amount of ECM matrix promotes cell migration and tissue repair[96]. The last stage of wound healing process is tissue remodelling where ECM components namely collagen rebuild the tissue and provide strength. Over the time, collagen fibers become more homogeneous to improve the tensile strength of the tissue[97].

Macrophages play a crucial role in the healing process. During the inflammatory phase, they are recruited to the wound site for cleaning up dead cells and protection of the site from infection. In the next stage (cell proliferation), they help developing new tissues and in the last one (tissue remodelling), they aid synthesizing the ECM[93]. Another key cell type in wound healing process responsible for deposition of extracellular matrix, fibers and secretion of growth factors are fibroblast cells of the connective tissues. Fibroblasts also differentiate to myofibroblasts that are in charge of synthesizing collagen[93]. Fibroblasts have two major functions in the wound contraction,

they alter the mechanical characteristics of the wound site and generate two key forces at the site, contraction and pulling of the tissue[98].

Fibronectin plays a crucial role during wound healing stages. At early stages, the wound is occupied with a clot containing Fn. Secreted Fn helps to form a clot. Due to many binding sites on Fn such as cell binding, Fn-Fn, Fn-Col and heparin binding sites, it promotes tissue repairing and cellular activities. In last stages of wound healing, dense fibrillar networks of fibronectin exist around fibroblasts, proving that fibronectin acts as a scaffold for cells to migrate during wound closure.

Beside fibronectin, collagen has a major role in wound healing sequence and promotes tissue regeneration and integrity as well as keeps the moist at the wound site[32]. The interactions between collagen I and Fn helps understanding role of collagen and Fn during wound healing process. It is shown that collagen I fibers colocalize with relaxed Fn fibers, suggesting that collagen fibers limit the stretchability of Fn fibers and prevent further unfolding. The presence of collagen I improves Fn fiber deposition while collagen I formation depends on Fn[53].

Studies have shown similarities in wound healing process and cancer. It has been declared that tumours emerge at severe untreated wound sites[99]. It was first found out that chickens developed cancer at the site of injection[100]. The clot that forms at early stages of wound healing contains several proteins such as fibrin and fibronectin. While fibrin and fibronectin network is one of the indications of cancer[101], another indication of cancer is the existence of excessive inflammatory cells which is one of the wound healing process stages (inflammatory)[102]. Although there are several similarities between wound healing and cancer, striking differences such as gene mutation lead to cancer progression[99].

1.5 Cancer Tissues

The main theory in cancer research is the ‘seed and soil’ hypothesis, which suggests that the microenvironment where cells reside (soil) is as important as the presence of cancer cells (seed). The environment can either promote or halt cancer progression. Considering this hypothesis, engineering tunable cell platforms helps understanding cancer invasion and metastasis[103]. The ECM plays a critical role in cell behaviour and survival. Not only it is crucial for cells to

differentiate and grow by providing biochemical and biomechanical signalling cues, also in cancer setting it might promote progression and create imbalances[66].

Fibronectin has shown significant roles in the cancer-associated extracellular matrix. Fn is overregulated and Fn fibers are stiffer and denser due to their unfolded conformation (as assessed by FRET). Changes in mechanical properties of Fn fibers affect consequent collagen I behaviour and promote increased collagen I deposition associated with tumour aggressiveness[104]. Also, it is found that there are no signs of Fn in tumours while Fn is ubiquitous in the neighbouring stroma[105,106].

Healthy and tumour microenvironments have shown significant differences in mechanical properties. The major sign of malignant tissues is abnormal growth and remodelling of stroma that result in increased stiffness. Stiffness has a major role in promoting cancer progression and metastasis[92]. In the normal ECM microenvironment, collagen fibers are curly and compliant while for instance in the neighbourhood of breast cancer cells, collagen fibers are abundant, thick, aligned in parallel bundles and stiff[107].

One of the key issues in cancer progression is vascularization through which blood and nutrients supplies flow and help tumour growth. Without vascularization, tumour growth would be stopped at size of 2-3 mm. One of the most prominent integrins, $\alpha_5\beta_1$, also called fibronectin receptor, promotes angiogenesis and is a pertinent therapeutic target. Fibronectin enhances angiogenesis by promoting vascular cells progression[108,109]. During tumour progression and cancer metastasis, ECM is constantly modified in terms of composition, morphology and stiffness. Altered ECM alters mechanosignalling, which results in tumour cell invasion and metastasis[110,111]. Alterations in vascularization due to ECM changes indicate cancer development. It has been shown that stiffer environment enhances collagen fibers alignment[90] suggesting that collagen fibers' alignment impact vascularization[91]. Balcioglu and coworkers have shown that the reorientation of collagen fibers and the change in the ECM over large areas were key factors leading to angiogenesis and metastasis. Hence, ECM properties including density and stiffness are crucial in promoting angiogenesis[112].

Although there has been a significant amount of research done already, there is still a clear need for complex and physiologically relevant 3D templates to be used as tunable matrix-mimicking

devices for long-term and large volume cell cultures for wound healing and cancer research purposes.

Chapter 2: Materials and Methods

2.1 Experimental Design

To engineer ECM-mimicking scaffolds two different approaches were utilized. In our first approach, 3D collagen 'porous' scaffolds were made via an ice-templating technique, which allowed us to control scaffold pore size and stiffness through collagen concentration and rate of freezing. These scaffolds were then coated with fibronectin using various thermal gradients to control Fn conformation (as assessed by Forster resonance energy transfer (FRET) spectroscopy). In our second approach, collagen-fibronectin 'fibrillar' scaffolds were engineered via a cold to warm casting technique, which provided better ECM-mimicking scaffolds. In both cases, cell behaviour such as cell invasion, adhesion, viability and proliferation were investigated.

2.1.1 Source of Collagen

Microfibrillar bovine Achilles tendon-derived collagen I and soluble rat-tail collagen I were used to fabricate porous collagen scaffolds and fibrillar collagen scaffolds, respectively.

2.1.2 Source of Fibronectin

Human plasma fibronectin (Invitrogen, Thermo Fisher Scientific) was diluted in 1x phosphate buffered saline (PBS) at concentration of 1 mg/ml for stock solution, and thereafter depending on the desired concentrations to coat porous scaffolds and to deposit fibronectin fibers in 3D collagen networks.

2.1.2.1 Fibronectin FRET Labelling

Fibronectin (Life Technologies, NY) was randomly single labeled with AlexaFluor 633 succinimidyl ester (Invitrogen, CA).

AlexaFluor 488 succinimidyl ester as FRET donor and AlexaFluor 546 malemide (Invitrogen, CA) as FRET acceptor were used to dual- label fibronectin as previously described by Smith and colleagues[36].

2.1.3 Source of Cells

One of the most common cell lines used in tissue engineering research are fibroblasts due to their ability to deposit matrix. 3T3-L1 cell line (representative of stromal cells), derived from mouse 3T3 cells were used in our experiments. To visualize cells, green fluorescent protein (GFP) labeled 3T3 cells were used.

2.2 Cell Culture

To study cell adhesion and attachment 3T3-L1 cells (ATCC #CL-173), an adipogenic subtype of mouse fibroblasts were used. Cells were incubated inside Dulbecco's Modified Eagle's Medium (DMEM) (Sigma Aldrich) including 10 vol% fetal bovine serum (FBS, Tissue Culture Biologics) and 1 vol% penicillin/streptomycin (Life Technologies) under 37°C and 5% CO_2.

2.3 FRET Data Acquisition

Samples were imaged with a Zeiss LSM 880 confocal microscope (Zeiss, Munich, Germany) using plan apochromat 20x/0.8 and plan apochromat oil-immersion 63x/1.4 objectives, a pinhole of 1 AU, a 488 nm laser set at 2% power to capture 12 bit z-stack images with a space of 3 μm. To acquire FRET-Fn images signals from PMT1 channel (514-526nm), the donor fluorophores, and PMT3 channel (566-578 nm), the acceptor fluorophores, were collected simultaneously.

2.4 FRET Data Processing

To analyze FRET images, mean dark current background values were subtracted from donor and acceptor images. Also, a threshold around 100 intensity was implemented on both donor and acceptor images. Then FRET images were analyzed quantitatively, pixel-by-pixel with an in-house Matlab code

to produce colour-coded FRET ratio (I_A/ I_D) images and histograms. High FRET ratio (yellowish pixels) indicates close-to-compact fibers while low FRET ratio (blue pixels) shows tumour-associated, unfolded fibers.

2.5 Data Analyzing

To analyze cell behaviour including cell adhesion and proliferation, cells were counted per each stack using Fiji is just ImageJ (Fiji). Averaged number of cells per each image was calculated and reported in millimetre cube.

2.6 Statistical Analysis

Results are shown as an average ± standard deviation and were analysed by one-way ANOVA in GraphPad Prism (GraphPad Software, California USA). If treatment level differences were determined to be significant, pair-wise comparisons were performed using Tukey's post hoc test and Student's t-test.

Chapter 3: 3D Fibronectin-coated Collagen Porous Scaffolds

3.1 Introduction

Studies have shown that cell behaviour on 2D or within 3D substrates are significantly different due to the complexity of 3D environments[113]. 3D biomedical scaffolds provide a better (more physiologically relevant) ECM mimicking environment for cells. They are used to replace or repair damaged tissues. Porous scaffolds promote cell invasion and nutrients flow through interconnected pores[114,115,116]. One popular class of biomaterials used as scaffolds are natural materials such as proteins due to their biocompatibility[68,117].

Collagen I is considered as one of the fundamental natural materials in terms of biodegradability, biocompatibility and mechanical characteristics. There are several common techniques to fabricate porous scaffolds such as freeze-drying which is an ideal technique to engineer protein-based scaffolds[118]. Fibronectin is one of the most crucial proteins in the ECM with major roles in several stages of wound healing process. Fibronectin conformation could change by cell traction, which in turn influences cell signalling[98,119]. Conformational changes can be traced using fluorescence resonance energy transfer (FRET).

In this chapter, properties of porous collagen scaffolds such as cell adhesion and invasion were investigated. To enhance biocompatibility of our porous scaffolds and gain control over protein conformation, we coated a layer of fibronectin on top of the collagen. It has been reported that Fn conformation is sensitive to temperature[59], so our collagen scaffolds were incubated with Fn solutions using various thermal gradients and the changes in Fn conformation were monitored using FRET. 3T3-L1 fibroblast cells were seeded on top of the scaffolds. The effect of Fn conformation on (i) scaffold cell invasion, (ii) cell adhesion, and (iii) cells' ability to deposit their own matrix were studied as they potentially all affect the wound healing sequence.

3D collagen porous scaffolds were fabricated initially using ice-templating technique. Collagen water-soluble suspensions of various concentrations were frozen under -10°C producing ice crystals. The latter were sublimated due to the reduction in chamber pressure, which resulted in porous structures of controlled pore size, pore interconnection, and mechanical stiffness.

3.2 Materials and Methods

3.2.1 3D Porous Collagen Scaffolds Fabrication

Porous collagen scaffolds were made by Yifan Li (earlier MSc student in the Gourdon group) using a previously published ice-templating technique[87]. Briefly, bovine-derived Achilles tendon (Advanced BioMatrix) collagen I was dissolved in 0.05 M acetic acid solution (Sigma-Aldrich) with 0.5, 0.75, 1.0 and 1.25 wt.% concentration and the pH were set to 2.0 with hydrochloric acid (VWR International). The suspension was blended with an overhead homogenizer (T 10 BASIC S001) for 30 minutes. Prior to placing samples into a freeze-dryer, the solution was casted into two engineered rectangular Teflon molds with the dimension of 10 × 7 × 2 mm^3 (l ×w × h). Then samples were frozen inside a freeze dryer (VirTis Advantage Plus ES; SP Scientific; PA, USA) at -10 °C for 5 hours and dried at the same temperature under 10 mTorr for 24 hours. In order to improve the stability of scaffolds, samples were chemically cross-linked using carbodiimide. Collagen scaffolds were immersed into 95% ethanol with 33 mM 1-ethyl-3-(3-dimethylamino propyl)-carbomiide hydrochloride (EDC) (Sigma Aldrich) and 6 mM N-hydroxysuccinimide (NHS) (Sigma Aldrich) for 4 h at 25°C. Samples were washed with distilled water and were placed inside the freeze-dryer again and the same process was applied.

Pore sizes in collagen scaffolds were adjusted by changing the concentration of collagen. Porous collagen scaffolds with concentration of 1.25 wt.% were used in all experiments in this thesis. All physical properties of scaffolds were measured by previous students as following: average pore diameter of 35.990 µm, total pore area of 2.103 m^2/g and compressive modulus of 1720 ± 300 Pa. 1.25 wt.% collagen scaffolds were chosen for use due to their best cell viability, adhesion and invasion compared to other scaffolds with different collagen concentration previously tested.

3.2.2 Cell Culture

To study cell adhesion and attachment 3T3-L1 cells (ATCC #CL-173), an adipogenic subtype of mouse fibroblasts was used. Cells were maintained in Dulbecco's Modified Eagle's Medium (DMEM) (Sigma Aldrich) supplemented with 10% fetal bovine serum (FBS) (Tissue Culture Biologics) and 1% penicillin/streptomycin (Life Technologies) at 37 °C in a humidified atmosphere under 5% CO_2, and passaged twice a week using standard techniques.

3.2.3 Cell Culture Experiments

Prior to use for our experiments, all scaffolds were cut into 1 mm thick samples and were put under UV light for 30 minutes for sterilisation. Clean scaffolds were then placed inside Nunc™ Lab-Tek™ 8 well chamber slides and washed with PBS three times. All samples were then coated with 30 µg/ml fibronectin either at 4°C or 37°C for 24h before being washed with PBS and moved to another well. Afterwards, 20 µl of cells with density of 30 thousand cells per well were seeded on top of each scaffold and were allowed to adhere. After an hour, fresh media containing 1 vol% FBS and 50µg/ml Fn of which 10% was FRET-labelled Fn was added to wells. Samples were incubated for 24 hours and were fixed in 3.7% cold paraformaldehyde (Sigma Aldrich). Cells nuclei were stained with 4′,6-diamidino-2-phenylindole (DAPI) (Life Technologies) to visualize cells. To study cell viability and penetration, green fluorescent protein (GFP) labeled 3T3 cells were used.

3.3 Results and Discussions

It was previously shown that 1.25 wt.% collagen scaffolds showed uniform pore sizes throughout the scaffolds and supported cells better, in terms of cell viability and invasion. Results showed that by increasing collagen concentration, cell invasion increased with a higher uniformity in pore sizes throughout the scaffold. Therefore, the 1.25 wt.% collagen scaffolds were used throughout this thesis.

3.3.1 Effect of Temperature on Fibronectin Conformation

In this study, the effect of temperature on Fn conformation was utilized to modify the surface of our collagen scaffolds. Briefly, collagen porous scaffolds were immersed in Fn solution under different temperatures and Fn conformation was assessed via intramolecular Forster Resonance Energy Transfer (FRET) imaging. Scaffolds were placed inside 8-well chamber slides and rinsed in PBS three times. Then, 0.05 mg/ml Fn solution in PBS (of which 10% was FRET labeled Fn) was added to the wells. One batch of scaffolds were placed inside the fridge (at 4°C) and another batch was placed in the incubator (at 37°C) for 24 hours. Prior to imaging, scaffolds were washed thoroughly with PBS. The data presented in (Figure 3.1) shows different Fn conformation on porous scaffolds in different coating temperatures. Fn coated at low temperature (4°C) were closer to compact conformation with high FRET ratios. At high temperature (37°C) Fn molecules were closer to unfolded conformation with low FRET ratios. These findings are consistent with previous results reported by our group on 2D surfaces, which further demonstrates our ability to tune Fn conformations using temperature gradients in both 2D and 3D environments.

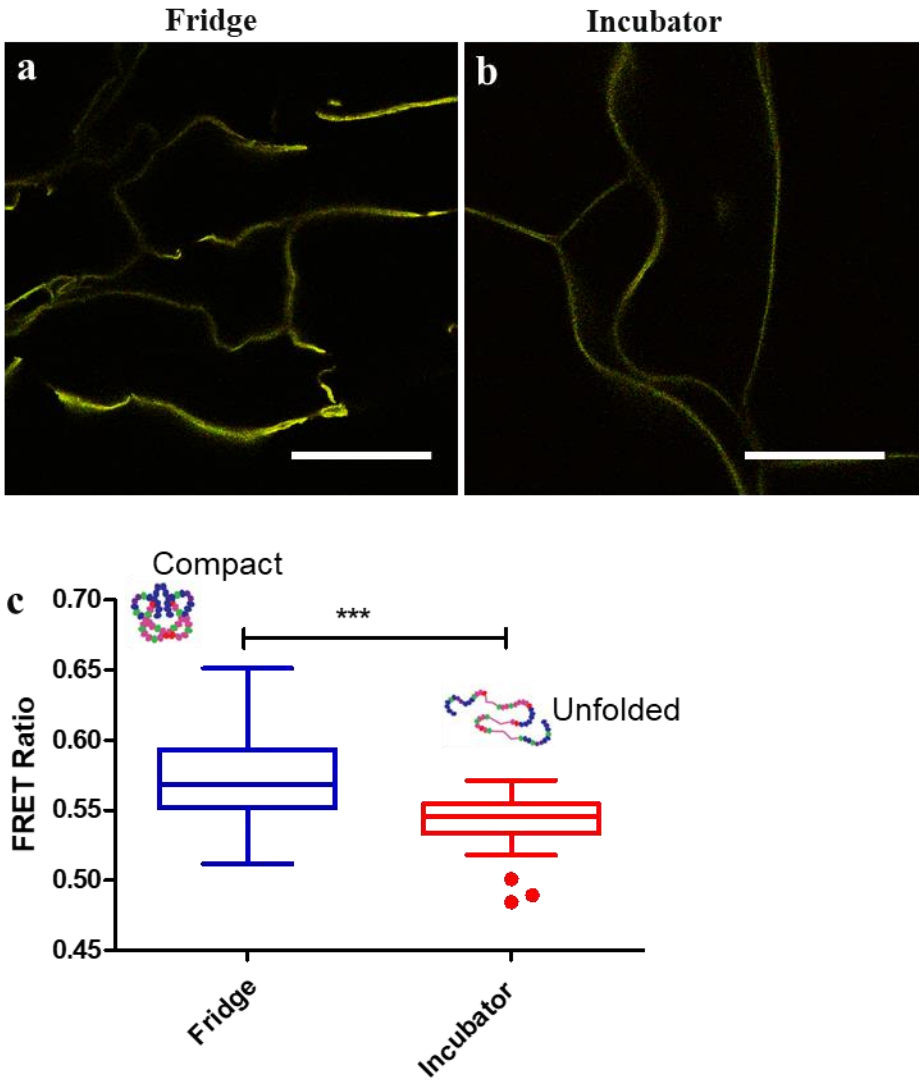

Figure 3.1 **Fibronectin conformation on collagen scaffolds**. Collagen scaffolds were coated with 0.05 mg/ml Fn of which 10% FRET kept in (a) the fridge (4°C) and (b) incubator (37°C) for 24 hours. Images were taken with a confocal Zeiss LSM 880 microscope using ZEN 2 .3 SP 1. FRET Fn was double labeled using AlexaFluor 488 and AlexaFluor 546. Signals were acquired from PMT1 channel (514-526 nm) and PMT3 channel (566-578 nm), the donor fluorophores and the acceptor fluorophores respectively. (c) Acquired FRET Fn Images were analyzed pixel by pixel with an in-house Matlab code to measure FRET ratio (IA/ ID). This shows that mean FRET ratio intensity was higher on Fn-coated scaffolds at 4°C (n=22) averaging around 180 measurements per sample, indicating close-to-compact Fn fibers while at 37°C (n=21), averaging around 170 measurements per sample, FRET ratio intensity was lower representing unfolded Fn fibers. The two groups are significantly different (***P<0.0001, Student's t-test). Mean ± SD. Bar=50 μm.

3.3.2 Effect of Fibronectin Conformation on Cell Adhesion and Invasion

Whether fibronectin conformation would enhance cell adhesion and invasion was studied by controlling its conformation on collagen scaffolds. Porous scaffolds were coated with unlabeled Fn and placed in the fridge (4°C) and the incubator (37°C) as described in the previous section with a control sample immersed in PBS at room temperature for 24 hours. Due to the importance of fibroblast cells in wound healing process, migrating and depositing matrix at the wound site, GFP 3T3 cells were used in this experiment to study cell invasion and adhesion. 30 k GFP-3T3 cells were seeded on top of scaffolds, then fresh media supplemented with 10% FBS was added to wells after an hour. Scaffolds were incubated for 24 hours. Images in Figure 3.2A-C show the distribution of cells into the different scaffolds and the total number of cells adhered on scaffolds were evaluated using Fiji. There are a few methods to quantify number of cells in the scaffolds. Cells could be trypsinized and collected in a vial. Then a viable cell count could be obtained using the hemocytometer and then normalized by scaffold volume to approximate cell density. This method would not be accurate here since not all of the scaffolds had the same volume. Manually quantifying cell density seemed to be a good estimation of cells in our experiments. In order to count cells, circa ten fields of views per scaffold were imaged randomly then cells were counted manually and number of cells in the volume were calculated and reported. The data show that cells prefer to invade (and interact with) Fn-coated collagen scaffolds placed in the fridge (4°C) compared to scaffolds in the incubator (37°C) and to the control samples, which was without Fn (Fig 3.2 D). Since collagen scaffolds were coated with Fn using two different temperature (4°C and 37°C), it would be expected to have two control samples without Fn, one kept at 4°C and another at 37°C. Although it has been shown that temperature might affect collagen molecules[120,] it is unlikely that it could affect the networks of our porous collagen scaffolds as they were already chemically crosslinked prior to incubation with Fn. Hence, only one control sample was used at room temperature. This can be explained by the more compact conformation (higher FRET ratio) of the Fn layer achieved at low temperature (fridge, 4°C) on top of the collagen scaffold, which likely favours adhesion of the 3T3 cells with Fn. These findings agree with our other previous work. The most common type of integrins 3T3 cells utilize to attach to substrates (and more specifically to Fn) are $\alpha_5\beta_1$ integrins[121]. However, it is believed that both the RGD loop (located on Fn III_{10}) and another binding sequence called the synergy site (located on adjacent Fn III_9) need to be engaged simultaneously by $\alpha_5\beta_1$ integrins to provide firm and long-lasting adhesion[122,123]. When Fn is nearly

unfolded, which is the case at high temperature, this dual involvement less probable due to the increased distance between Fn III_{10} and Fn III_9. As a consequence, cells need to use other integrins such as $\alpha_V\beta_3$ that attach only to RGD loop, which results in weaker binding.

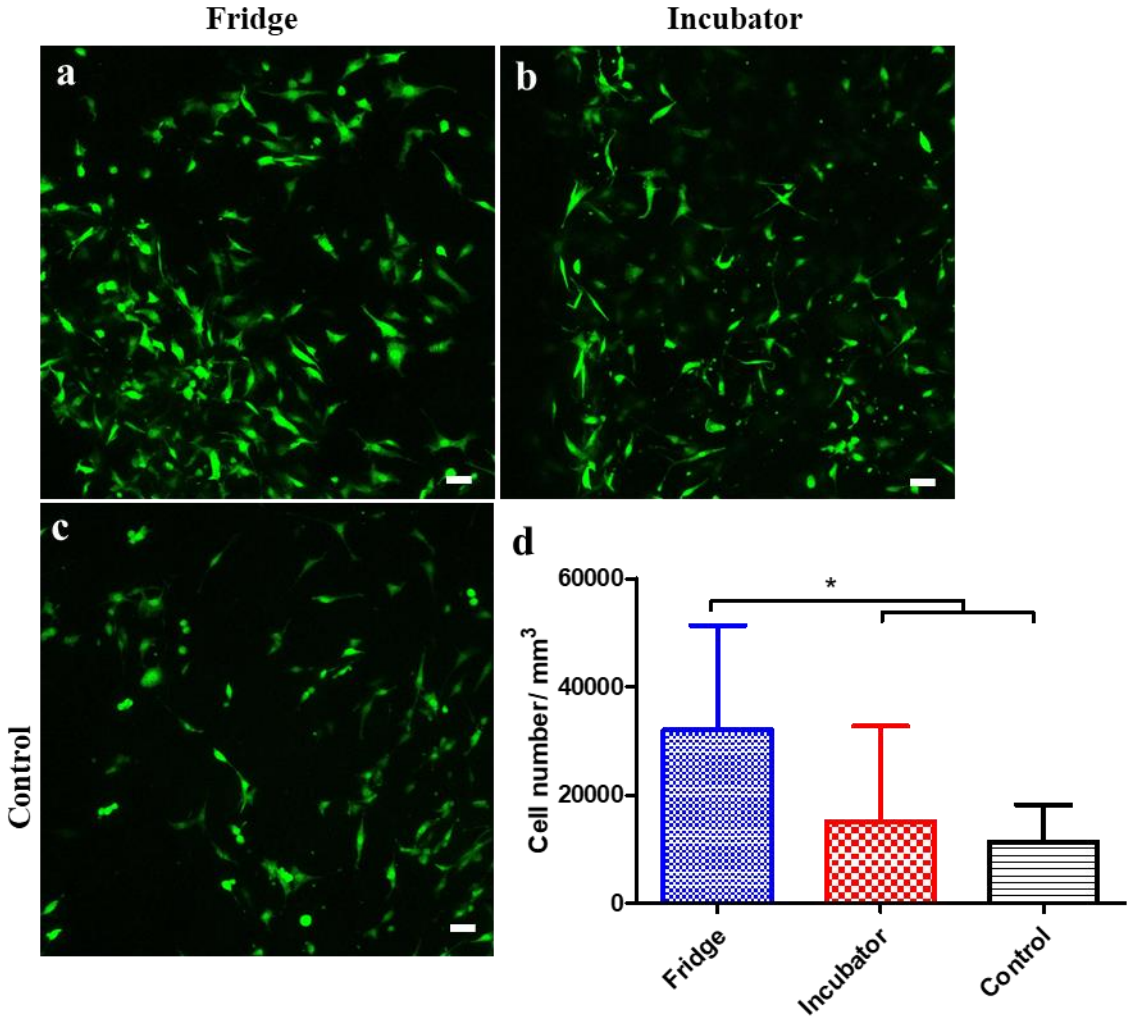

Figure 3.2 **Effect of Fn conformation on cell adhesion**. 0.03 mg/ml Fn was coated on porous collagen scaffolds and placed in (a) fridge (low temperature) (n=11), averaging around 170 points measurements per sample, and (b) incubator (high temperature) (n=13), averaging around 200 points measurements per sample, for 24h. (c) Control scaffolds were kept in PBS at RT (n=6), averaging around 90 points measurements per sample. The scaffolds were seeded with 30k GFP-labeled 3T3 cells in DMEM supplemented with 10% FBS and incubated for 24h, after which samples were fixed with 3.7% paraformaldehyde and imaged with a confocal Zeiss LSM 880 microscope using ZEN 2.3 SP 1. (d) Cells were counted using Fiji and showed that number of cells in Fn-coated scaffolds placed in the fridge were higher than scaffolds in the incubator and the

control samples (without Fn). The groups are significantly different (*P< 0.05, using one-way ANOVA with Tukey's post hoc). Mean ± SD. Bar=50 μm.

Cell invasion data (Figure 3.3) show that cells were able to infiltrate the Fn-coated collagen scaffolds up to 400 μm in depth. Our results indicate that collagen scaffolds represent a proper 3D environment for cells to attach and grow, which is a prerequisite of 3D ECM mimicking template for long-lasting cell cultures over large volumes. It is shown that despite the fact that cells invaded Fn-coated collagen scaffolds placed in the incubator (37°C), most cells were adhered to the first 100 μm of scaffolds. On the contrary, most cells in Fn-coated collagen scaffolds placed in the fridge (4°C), were adhered to at a depth of approximately 200 μm. Meanwhile, cell distribution was more uniform through the control sample (data not shown here).

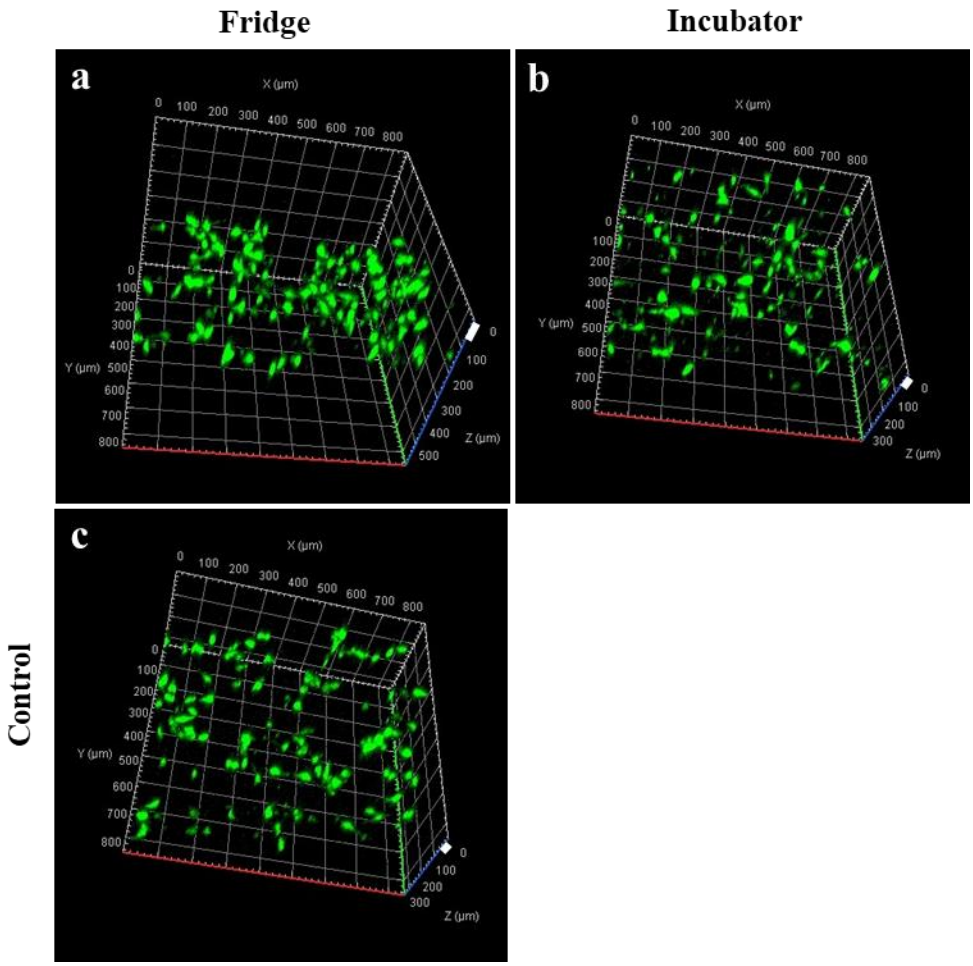

Figure 3.3 **Effect of Fn-coated conformation on cell invasion.** 0.03 mg/ml Fn was coated on porous collagen scaffolds and placed in (a) fridge (low temperature) (n=11), averaging around 170 points measurements per sample and (b) incubator (high temperature) for 24h (n=13), averaging around 200 points measurements per sample. (c) Control scaffolds (n=6), averaging around 90 points measurements per sample, were kept in PBS at RT, 3D immunofluorescence. The scaffolds were seeded with 30k GFP-labeled 3T3 cells in DMEM supplemented with 10% FBS and incubated for 24h, after which samples were fixed and imaged as in previous figures. (D) Cells number was quantified per each 10 µm using Fiji and showed that scaffold provided proper environment for cells to invade almost 400 µm which proved scaffolds' biocompatibility. Bar=50 µm.

3.3.3 Effect of Fn Conformation on Cell-deposited Matrix

As shown above, cells are highly sensitive to the biochemistry of their substrates (in particular to the underlying protein conformation), which not only affects their adhesion and invasion response but also alters both the amount and the conformation of the matrix they deposit[51,124,125].

Here we first assessed the ability of two cell lines (C_2C_{12} and 3T3-L_1) to deposit their own Fn matrix on 2D substrates. 8-well chambered coverglass were coated with 0.03 mg/ml unlabeled Fn at room temperature for 1 hour prior to seeding with 100k C_2C_{12} or 3T3-L_1 cells per well and incubated for 24 hours. Figure 3.4 shows the ability of C_2C_{12} and 3T3-L_1 cells to deposit their own Fn matrix in 2D environments. It was visually observed that the Fn fibers deposited by 3T3-L1 were longer. No further analyses were conducted on 2D results to measure the difference, if any, between the cell-deposited matrix. 3T3-L1 cells were chosen for seeding on the scaffolds as a model for stromal cells behavior such as adhesion, proliferation and their further effect on wound healing process.

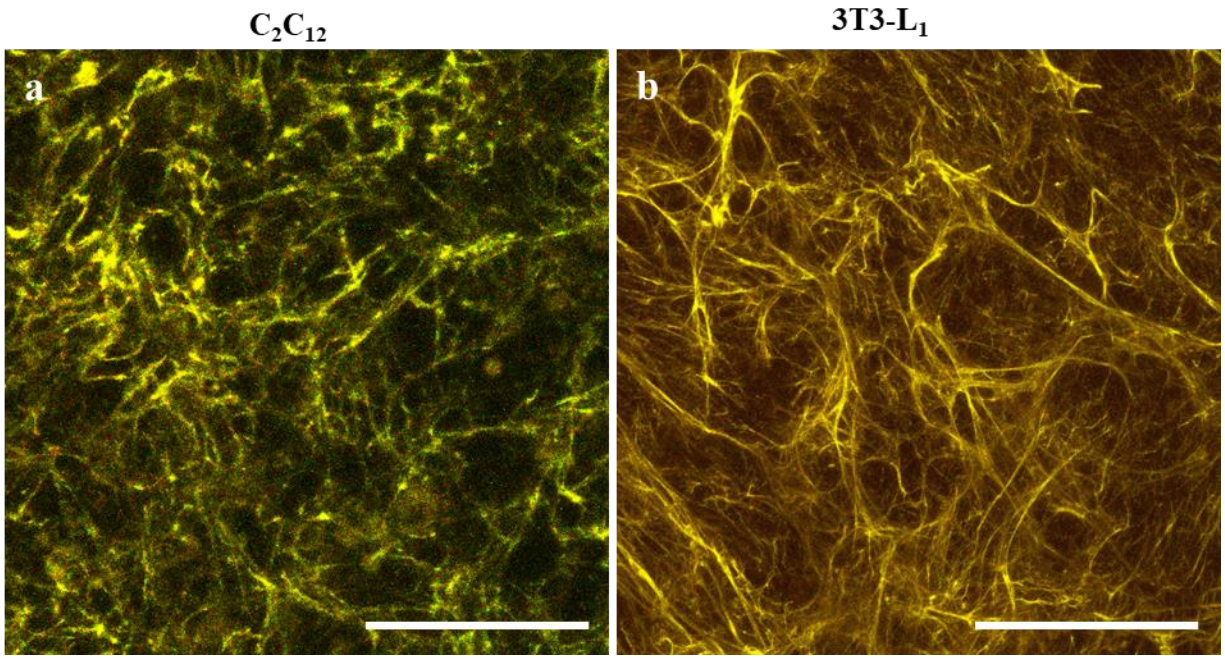

Figure 3.4 **Cell matrix deposition on coverglass.** 100 k (a) C2C12 and (b) 3T3-L1 cultured in 8-well chambered coverglass. Wells were coated with 0.03 mg/ml Fn for 1h at RT prior to cell seeding in DMEM containing 10% FBS. After 1h, new DMEM containing 10% FBS and 0.05 mg/ml Fn of which 10% was FRET Fn was added and samples were incubated for 24 hours. FRET ratio images were taken after fixation and modified with Fiji by maximum projection. The FRET signal proved that both C_2C_{12} and 3T3-L_1 were able to deposit fibronectin. Bar=50µm.

Next, we studied whether cells could make their own matrix within the pores of our 3D Fn-coated collagen scaffolds. 50k 3T3 cells per well were seeded on top of Fn-coated scaffolds in DMEM media containing 1% FBS. After an hour, DMEM media containing 1% FBS and 0.05 mg/ml Fn of 10% which was single-labeled Fn (AlexaFluor 546) was added to the wells. Scaffolds were incubated for 24 hours after which they were fixed prior to imaging. The nuclei were stained with DAPI.

Figure 3.5 shows 3T3-L1 cells were able to perform some regular cell functions, in particular cell spreading and matrix deposition inside the collagen scaffolds suggesting the biocompatibility of the scaffolds which supports cell functions. It is shown that fibers are mostly seen between pores and around isolated cells. The circled areas show cell-deposited Fn between the pores. Visually there is no difference between deposited matrix in the two conditions. Quantity of deposited Fn was not measured by any means.

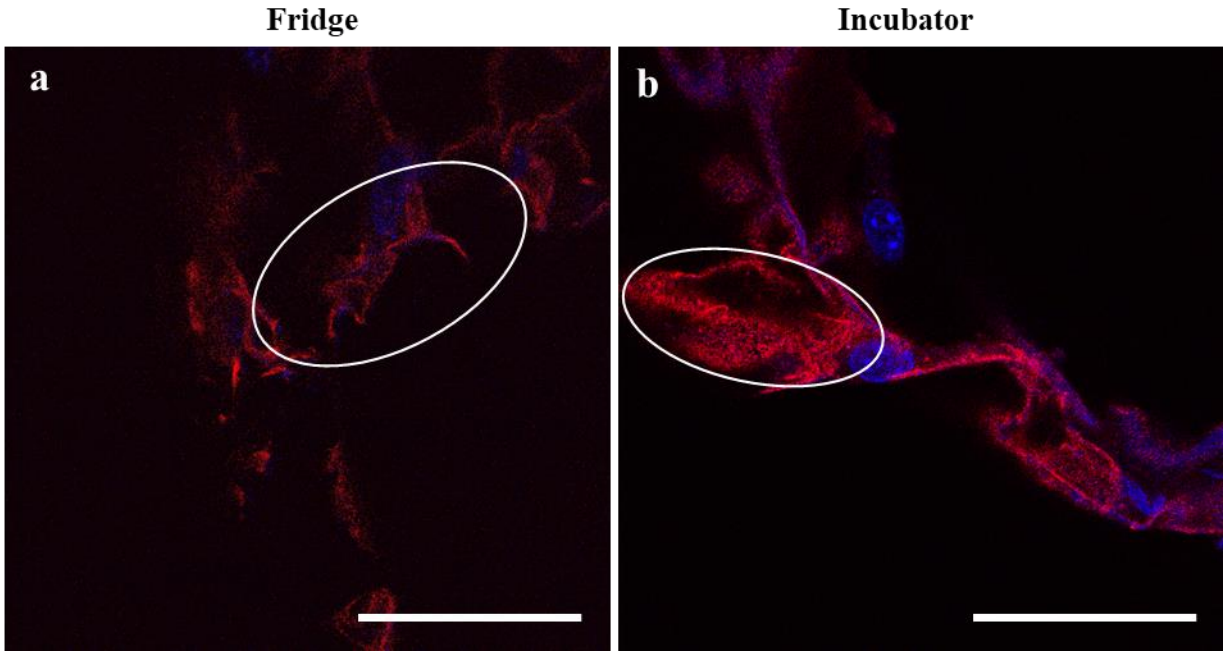

Figure 3.5 **3T3-L1 matrix deposition on collagen scaffolds** after 24h cultured in DMEM 1% FBS. Scaffolds were coated with 0.03 mg/ml Fn and placed in (a) the fridge or in (b) the incubator for 24h prior to seeding with 50k 3T3-L1 cells on top of the scaffolds. DMEM containing 1% FBS and 0.05 mg/ml Fn of which 10% was single labeled Fn was added after 1 h. Scaffolds were fixed and nuclei were labeled with DAPI. The images show that cells deposited Fn fibers inside the 3D collagen scaffolds. Bar=50 µm.

To determine whether the conformation of the Fn coating of the porous collagen scaffolds affected the conformation of matrix deposited by the infiltrated cells, we repeated the previous experiment with FRET-labelled Fn to quantify the conformation of cell-made Fn fibers. As described previously, collagen scaffolds were coated with Fn and placed either in the fridge (4°C) or in the incubator (37°C). 50k 3T3 cells were seeded per well on top of scaffolds in DMEM media containing 1% FBS. After an hour, medium was added containing 1% FBS and 0.05 mg/ml Fn of which 10% was FRET-labelled and the scaffolds were incubated for 24h. Cell-made matrix was observed inside pores and around isolated cells (Figure 3.6A-D). The data show close-to-compact (higher FRET ratio) cell-deposited Fn in scaffolds initially placed in the fridge compared to close-to-extended (lower FRET ratio) cell-deposited Fn initially placed in the incubator (Figure 3.6E). Collectively, our findings indicate (i) that we were able to engineer 3D ECM-mimicking platforms in which only one parameter (here Fn conformation) can be tuned while all others parameters (scaffold rigidity, pore size, pore connectivity etc.) are kept constant, (ii) that cells could sense the

underlying Fn conformation of the scaffold coating and (iii) that cells respond to these changes by depositing matrix fibers exhibiting different molecular conformation (at least at 24h). Wang and coworkers have shown that 3T3-L1 cells on 2D substrates with the presence of collagen and fibronectin, deposited close-to-compact and extended Fn conformation matrix after 24h of culture, which is consistent with our results[104].

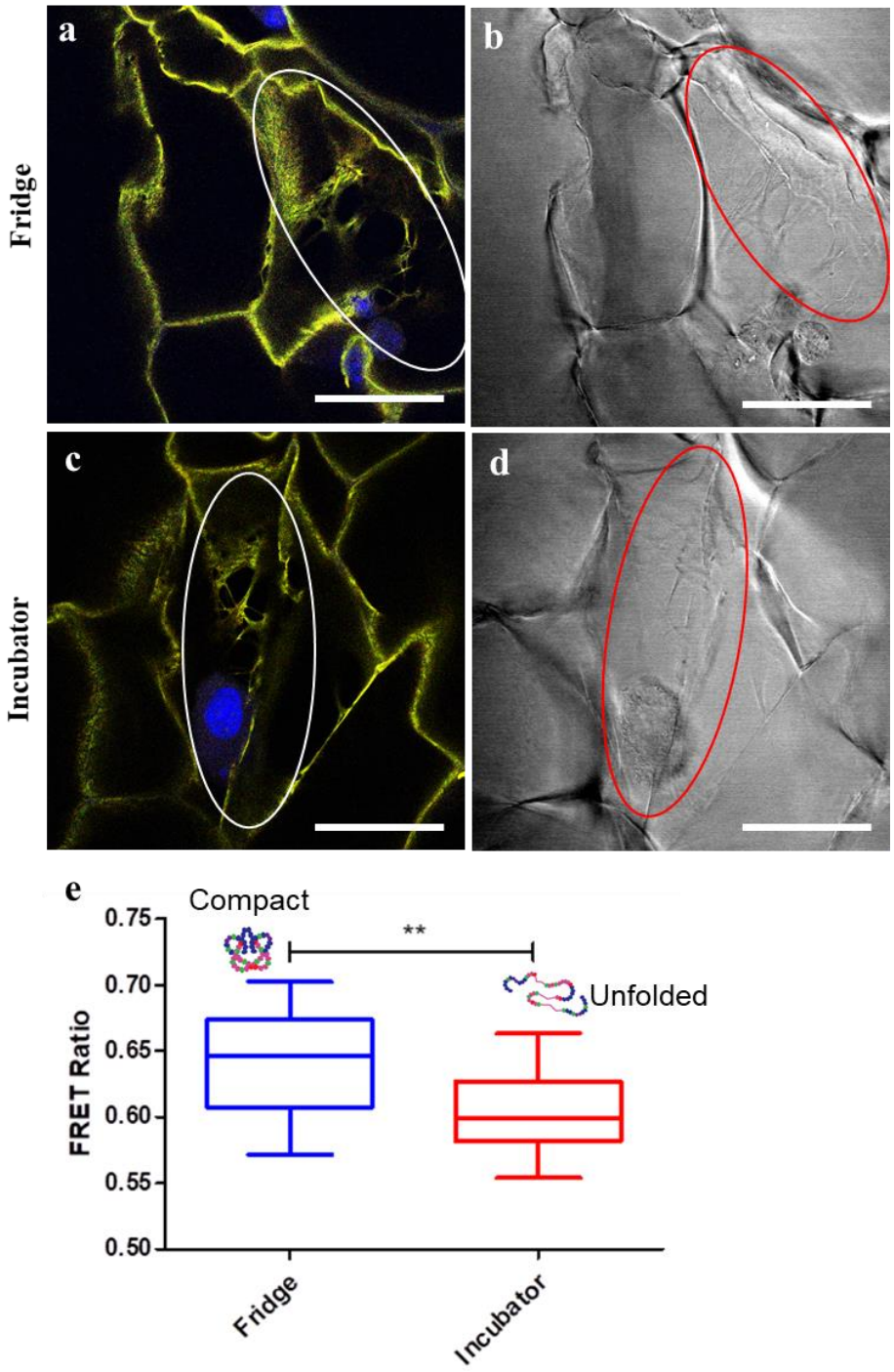
a
b
c
d
Fridge
Incubator
e
Compact
Unfolded
**
FRET Ratio
0.75
0.70
0.65
0.60
0.55
0.50
Fridge
Incubator

Figure 3.6 **Analysis of the conformation of cell-deposited matrix**. Scaffolds were coated with 0.03 mg/ml Fn and placed in the fridge (a, Immunofluorescence image (a combination of FRET ratio and DAPI staining); b, DIC image) or in the incubator (c, Immunofluorescence image (a combination of FRET ratio and DAPI staining); d, DIC image) for 24h prior to seeding with 50k 3T3-L1 cells on top of scaffolds in DMEM containing 1% FBS. After 1h, DMEM containing 1% FBS and 0.05 mg/ml Fn on which 15% was FRET Fn was added. (e) Images were analyzed pixel by pixel with an in-house Matlab code to measure FRET ratio (IA/ ID). This shows that mean FRET ratio intensity is higher for scaffolds in the fridge (4°C) (n=18), averaging around 70 points measurements per sample which indicates close-to-compact Fn fibers while for scaffolds in the incubator (37°C) (n=23), averaging around 80 points measurements per sample, it indicates lower FRET intensity ratio meaning unfolded Fn fibers. The two groups are significantly different (**P<0.001, Student's t-test). Mean ± SD. Bar=50 μm.

3.4 Conclusions

In this chapter, porous scaffolds with collagen concentration of 1.25 wt.% were used. These collagen scaffolds were coated with a fibronectin layer using various incubation temperatures allowing us not only to improve overall cell-scaffolds interactions but also to tune the scaffolds surface characteristics (here Fn conformation) to study the effect of Fn conformation on cell behaviour.

Our FRET data indicated that the conformation of Fn decorating the pores of the collagen scaffolds can be switched from compact to unfolded when the incubation temperature is changed from 4°C to 37°C, respectively. This Fn conformation switch consequently affects not only overall cell adhesion and viability (higher adhesion and viability when Fn coating of scaffolds is compact) but also later cell deposition of ECM (more ECM of more compact conformation when initial Fn coating of scaffolds is compact).

Here, we show that, by tuning the conformation of the Fn coating on collagen scaffolds and by keeping constant the overall stiffness of the bulk scaffold, we are able to control the conformation of early deposited matrix, which has potentially tremendous impact on both the first stages of wound healing and the vascularization of tumours. Collectively our findings suggest that the scaffolds we engineered could be utilized as 3D model cell culture systems to study wound healing and control cell functions in both pathological and tumourous conditions.

The engineered porous scaffolds presented in this chapter were chemically cross-linked. Despite chemical crosslinking is a common method for hydrogels, physical crosslinking has been developed and applied for biomedical scaffolds due to chemical crosslinking limitations. Chemical agents are not usually biocompatible and they interfere with biological events such as cell behaviour. Also, they are usually toxic which in some cases need to be removed prior to their use. On the other hand, physical crosslinking has been focused on cell-embedded scaffolds especially while hydrogels polymerise under mild conditions by modifying temperature, pH or a specific compound where cells will be able to remodel the hydrogels[126]. Collagen scaffolds discussed in Chapter 4 were crosslinked using a temperature mediated method.

Paper (Asadishekari M., Li Y., Ye J., Ngandu Mpoyi E. and Gourdon D.* “3D tunable fibronectin-collagen platforms for control of cell adhesion and matrix deposition”) is in preparation for ACS Biomaterials Science and Engineering publications (October 2018).

Chapter 4: 3D Fibrillar Collagen-Fibronectin Scaffolds with Tunable Microarchitecture and Mechanical Properties

4.1 Introduction

The ECM has been shown to provide a support for cellular interactions in particular for cell adhesion, proliferation and survival[18]. As mentioned in the previous chapters, ECM structural, mechanical and biological characteristics play key roles in regulating cell functions. Biomechanical properties of the ECM such as stiffness as well as structural properties including porosity and overall morphology (pore connectivity, fiber thickness, length etc.) have been taken into account since they regulate cell behaviour such as cell signalling[127,128,129]. Collagen I (Col I) the most ubiquitous protein in the ECM along with fibronectin (Fn), one of the key proteins in the ECM, have been widely used to study cellular behaviour[130,131].

In cancer studies, the role of the tumour environmental ECM is considered as important as the existence of cancer cells that (reside in and) control tumour growth. Moreover, it is known that ECM in a context of cancer is dysregulated[104]. The tumour microenvironment exhibits considerable differences in terms of mechanics, structure and morphology compared to healthy tissues[132]. Collagen fibers in vicinity of tumour tissues are abnormally deposited, thick and reoriented suggesting stiff environment while in healthy tissues, collagen fibers are curly and thin suggesting compliant ECM networks[66,92,133].

It has been demonstrated that Fn is involved in early stages of tumour growth and metastasis. With the aid of FRET technique, it was shown that Fn in tumour tissues is denser, stiffer and more unfolded, which consequently induces altered collagen I deposition and tumor progression[66,104]. Collagen scaffolds of various micro–structures have been fabricated and studied in tissue engineering fields. To engineer collagen scaffolds, several parameters including pH, temperature, concentration and structure such as density, fiber diameter and length have been considered as they all control overall collagen scaffolds properties[92,134].

Fibroblasts interact with their surroundings and play an active role in collagen fibrillogenesis. They have three roles in morphogenesis: forming fibrils from collagen molecules, bundling collagen

fibrils and forming aggregates from collagen bundles[135,136,137]. Therefore, analyzing fibroblasts behavior in fibrillar scaffolds helps studying fibrillogenesis.

In this chapter, we first aimed to fabricate collagen scaffolds without chemical crosslinking as in Chapter 3 but using temperature-mediated methods to control the collagen polymerisation and tune the scaffolds' microstructure. In this way, we expect that cells will be able not only to invade the scaffolds but also to remodel them when proliferating. Next, we want to ensure that the scaffolds will have a genuine matrix mimicking morphology, namely that they will have a real 'fibrillar' structure instead of a 'porous' morphology as described in Chapter 3. Finally, we aim at incorporating Fn fibers of controlled conformation within the collagen scaffolds to (i) enhance scaffolds properties and (ii) tune their structure precisely using time and temperature. Cell behavior such as cell viability was also studied to test the biocompatibility of the collagen-Fn scaffolds.

4.2 Materials and Methods

4.2.1 Fibrillar Collagen Scaffolds

The 3D fibrillar scaffolds were made by mixing the neutralization solution with the rat tail collagen I solution (both from Advanced BioMatrix) in a 1 to 9 proportion (3.6 mg/ml), for a final volume of 150 µl per wells of 96-well plates to obtain around 1.0 mm thick collagen scaffold. All solutions were kept on ice. 96-well plates were either pre-cooled at -20°C for 1h or pre-warmed in the incubator for 1 h. Fibronectin was added to collagen solutions at different stages of the preparation to engineer better ECM-mimicking scaffolds. Collagen scaffolds with a final volume of 150 µl per well were prepared as a function of final collagen concentration of either 2.88 mg/ml (with final Fn concentration of 0.2 vol%) or 2.16 mg/ml (with final Fn concentration of 0.4 vol%). Fn was added to mixture and either injected into pre-cooled 96 well-plates to gradually polymerise under series of steps of temperature from 4°C (fridge for 15 mins) to RT temperature 22-24°C (for 15 mins) and into the incubator (37°C for 30 mins to polymerise), or injected into pre-warmed 96-wells and placed into the incubator for 1h to gelatinize. After 1h in the incubator, PBS was added to all the plates to prevent dry out. Scaffolds were incubated for 24h, fixed with 3.7% cold paraformaldehyde for 1h and washed three times with PBS prior to imaging.

In parallel, we also prepared 3D fibrillar scaffolds with pre-embedded cells to study cell distribution and cell-scaffolds interactions. For these, GFP labeled 3T3 cells (10 µl containing 100,000 cells) were added while mixing the collagen and neutralization solutions. The scaffolds contained into plates were processed as mentioned above and after polymerisation and gelatinization, DMEM including 10% FBS was added to wells and incubated for 24 hours. Scaffolds were fixed with 3.7% ice-cold paraformaldehyde prior to imaging.

4.3 Results and Discussions

4.3.1 Engineering of Fibrillar Collagen Scaffolds with Two Different Microstructures Using Warm/Cold Cast Technique

Collagen solution was added either to pre-cooled 96 well-plates and gradually warmed up to 37°C (cold cast) or to pre-warmed 96-well plates and warmed up rapidly (warm cast). Here, we used temperature to control fibrillar structure of scaffolds and monitor the rate polymerisation of collagen. The thermal gradient regulated fiber density as well as fiber thickness. Figure 4.1 shows the microstructure of cold-cast and warm-cast collagen scaffolds. It was observed that warm-cast scaffolds were significantly denser (average pore size ~ 10.23 μm^2) with smaller fiber thickness (average fiber thickness ~ 1.98 μm) and length (average fiber length ~ 5.46 μm) compared to the cold-cast scaffolds. Cold-cast scaffolds were less dense (average pore size ~ 183.18 μm^2) likely due to the reduction of nucleation events resulted in fewer interactions of monomers with polymers[92]. The fiber thickness of cold-cast scaffolds averaged ~ 2.83 μm and the length ~29.34 μm. Collagen fibers are clearly observed in the cold cast compared to the warm cast. This could be due to the fact that cold cast scaffolds were gelatinized gradually under thermal gradient from 4°C to 37°C, while in warm cast scaffolds collagen was quickly polymerised at 37°C resulting in a denser network. Since porous (hence less dense) scaffolds provide better microenvironment for cells in terms of cell interaction and nutrients flow, we concentrated on cold-cast collagen scaffolds in the next phase of our protocols.

Our results are in agreement with Staunton and coworkers who reported that scaffolds polymerised at 4°C showed longer, thicker and less dense fibers with larger pore size while at higher temperature (37°C) collagen fibers were short and formed a denser network, similar to a hydrogel[92]. Fn was incorporated into the 3D collagen scaffolds and the effect of both collagen concentration and Fn concentration on the scaffold microstructure were investigated.

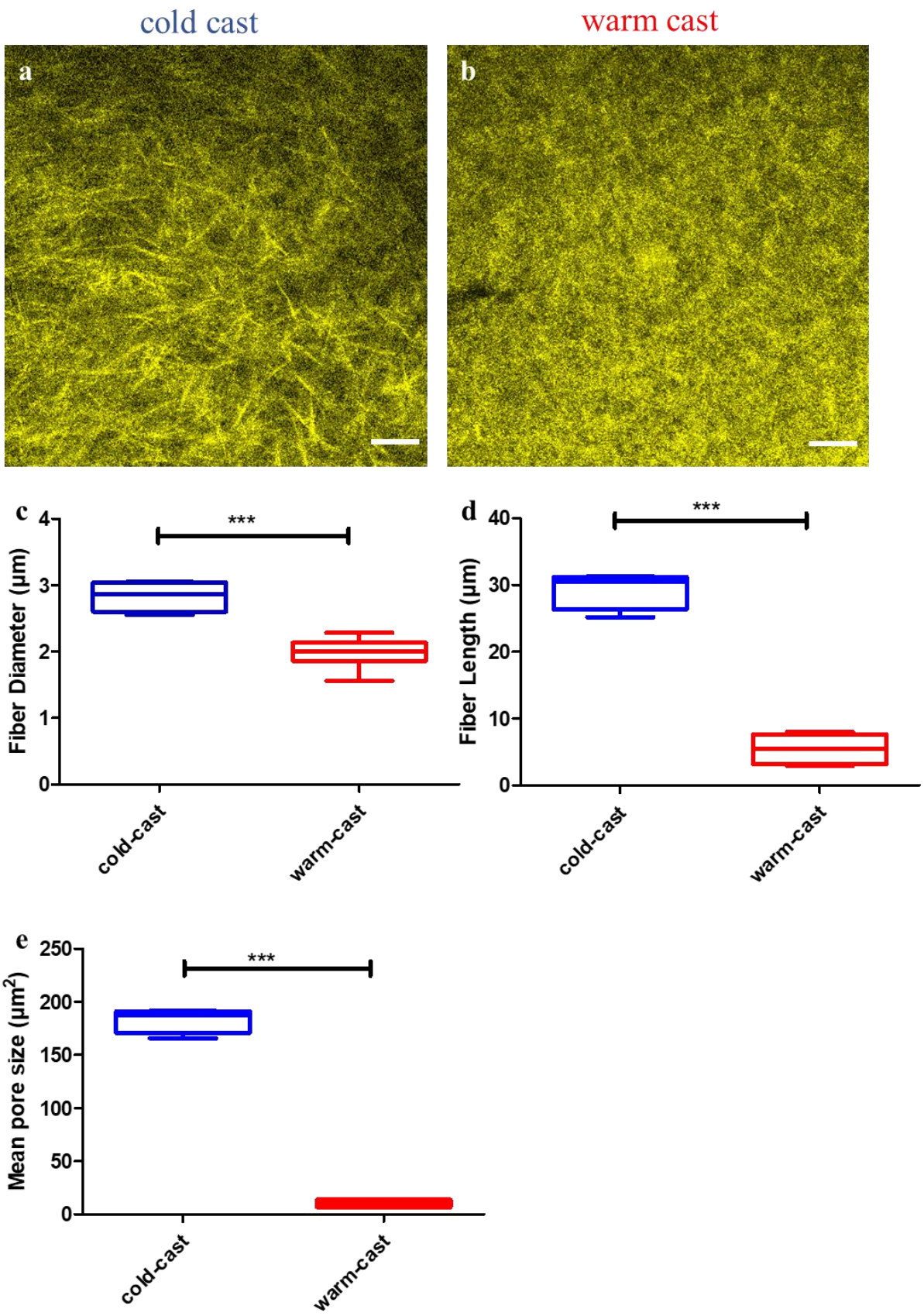
cold cast
warm cast
a
b
c
Fiber Diameter (µm)
0
1
2
3
4
***
cold-cast
warm-cast
d
Fiber Length (µm)
0
10
20
30
40
***
cold-cast
warm-cast
e
Mean pore size (µm²)
0
50
100
150
200
250
***
cold-cast
warm-cast

Figure 4.1 **Microstructure of 3D cold and warm-cast collagen scaffolds**. Reflectance confocal microscope (RCM) images of cold and warm-cast collagen scaffolds. (a) Cold-cast collagen scaffolds (n=3) averaging around 240 points measurements per sample: 96 well plates were pre-cooled at -20°C. After adding collagen solution at 3.6 mg/ml concentration, plates were gradually warmed up 15 mins at 4°C, 15 mins at RT and then 24h inside incubator (b) warm-cast collagen scaffolds (n=4) averaging around 290 points measurements per sample: 96 well plates were placed at 37°C for 30 minutes. After adding collagen solution at 3.6 mg/ml concentration, plates were incubated 24h inside incubator. (c) Average fiber diameter of cold cast (~ 2.83 μm) and warm cast (~ 1.98 μm) scaffolds. (d) Average fiber length of cold cast (~ 29.34 μm) and warm cast (~ 5.46 μm). (e) Average pore size of cold cast (183.18 μm^2) and warm cast (10.23 μm^2) scaffolds. Images were analyzed using Fiji. The data shows that warm-cast scaffolds were significantly dense with short collagen fibers compared to cold cast scaffolds. (***P<0.0001; Student's t-test). Mean±SD. Scale bars = 50 μm.

4.3.2 Cold-Cast Collagen-Fibronectin Scaffolds with Different Collagen Concentration

To improve biocompatibility, and to add a level of complexity to our biomimetics, and control protein conformation, fibronectin a key mechanotransducer protein in the ECM, was added to scaffolds. To determine the effect of collagen concentration on overall scaffolds microstructure, we designed two batches of scaffolds. First batch contained 2.88 mg/ml Col I concentration with 0.2 vol% Fn along with a control sample containing 0.2 vol% PBS and the second one contained 2.16 mg/ml Col I concentration with 0.4 vol% Fn along with a control sample containing 0.2 vol% PBS. Figure 4.2 shows the effect of Col I concentration on the microstructure of the resulting Col I - Fn scaffolds. Fiber diameter averaged ~ 2.14 μm for the 2.88 mg/ml collagen concentration scaffolds and ~ 2.26 μm for the 2.16 mg/ml scaffolds. Averaged fiber length for the 2.88 mg/ml collagen concentration scaffolds measured approximately 24.73 μm and 21.80 μm for the 2.16 mg/ml scaffolds. Mean pore area measured ~ 96.13 μm^2 for the 2.88 mg/ml collagen concentration scaffolds and ~ 120.82 μm^2 for the 2.16 mg/ml scaffolds. Comparing Col I - Fn scaffolds with the control samples (only Col I) suggested that adding Fn would not affect overall scaffolds microstructure. Moreover, when comparing scaffolds made of 2.88 mg/ml Col I with 0.2 vol% Fn and 2.16 mg/ml Col I with 0.4 vol% Fn, no significant change in the microstructure was noted although Fn concentration was almost doubled. To conclude, analysis proved that Col I concentration did not affect fiber microarchitecture such as fiber diameter, length and pore sizes. Once more, our results are consistent with previous observations that have demonstrated that

collagen concentration does not play a key role in overall scaffolds microstructure[92]. We therefore focused on Col I - Fn scaffolds with collagen concentration of 2.88 mg/ml and Fn 0.2 vol% for all consecutive experiments. To control fiber formation in our scaffolds, we explored the effects of Fn incubation time in the Col I mixture as well as temperature.

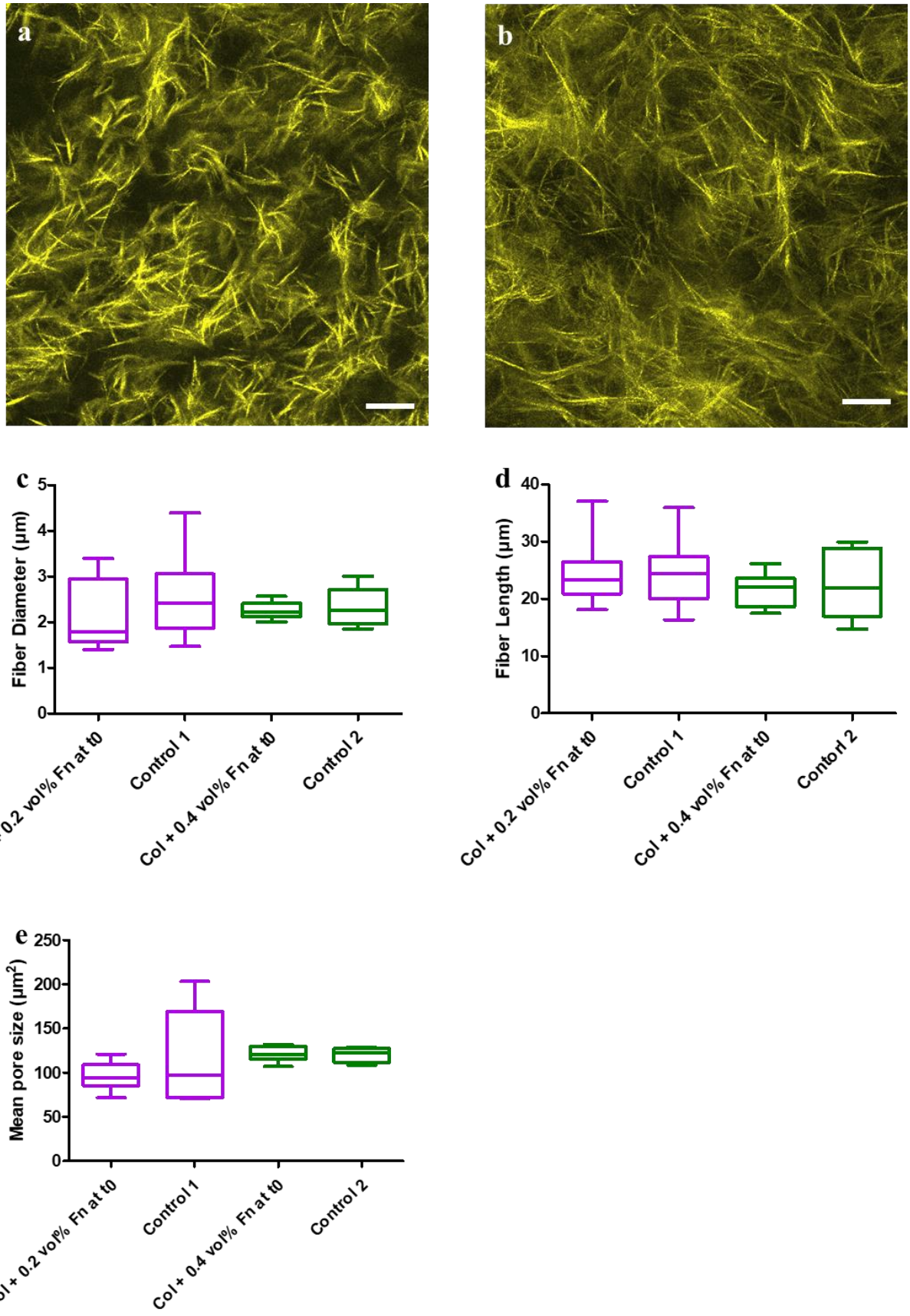
a
b
c
Fiber Diameter (µm)
0
1
2
3
4
5
Col + 0.2 vol% Fn at t0
Control 1
Col + 0.4 vol% Fn at t0
Control 2
d
Fiber Length (µm)
0
10
20
30
40
Col + 0.2 vol% Fn at t0
Control 1
Col + 0.4 vol% Fn at t0
Control 2
e
Mean pore size (µm²)
0
50
100
150
200
250
Col + 0.2 vol% Fn at t0
Control 1
Col + 0.4 vol% Fn at t0
Control 2

Figure 4.2 **Effect of collagen concentration on the microstructure of 3D cold-cast collagen-Fn scaffolds**. RCM images of collagen-Fn scaffolds with Fn concentration of (a) 0.2 vol% (b) 0.4 vol%. Collagen-Fn scaffolds were fabricated with two different concentration of 2.88 mg/ml (n=3), averaging around 240 points measurements per sample, and 2.16 mg/ml (n=4), averaging around 240 points measurements per sample, with two control samples of 0.2 vol% PBS (control 1) (n=3), averaging around 180 points measurements per sample and 0.4 vol% PBS (control 2) (n=3), averaging around 150 points measurements per sample. Images were analyzed in terms of fiber diameter and length using Fiji. (c) Average fiber diameter of collagen fibers when collagen concentration was 2.88 mg/ml = 2.14µm (0.2 vol% Fn), control 1 = ~ 2.60 µm, 2.16 mg/ml = ~ 2.26 µm (0.4 vol% Fn), control 2 = ~ 2.34 µm (d) average fiber length of collagen fibers when collagen concentration was 2.88 mg/ml = ~ 24.73 µm (0.2 vol% Fn), control 1 = ~ 25.29 µm, 2.16 mg/ml = ~ 21.80 µm (0.4 vol% Fn), control 2 = ~ 22.22 µm. (e) mean pore size of collagen fibers when collagen concentration was 2.88 mg/ml = ~ 96.13 μm^2 (0.2 vol% Fn), control 1 = ~ 117.77 μm^2, 2.16 mg/ml = ~ 120.82 μm^2 (0.4 vol% Fn), control 2 = ~ 120.51 μm^2. The data shows that collagen concentration didn't regulate fiber structure. (Student's t-test). Scale bars = 50 µm.

4.3.3 Tuning Fibrillar Collagen-Fibronectin Scaffolds Microstructure

In order to tune overall scaffold morphology, we explored the effect of incubation time of Fn with the Col I mixture during the gelation process. Several experiments were performed in which Fn solution was added at several time points t=0, t=15, t=30 and t=45 minutes. To track Fn molecules, 10% labelled Fn was added to unlabelled Fn solution and this was mixed with collagen solution and injected into pre-cooled wells while for 3 other batches only collagen was added to the wells. Results at t=0 and t=15 showed clear collagen fibers while at t=30 collagen scaffolds were semi-gelatinized and after 45 minutes of fabrication gels were completely polymerised (data not shown here). This indicates that, the longer we waited to add Fn, the harder it was to mix it properly with collagen as scaffolds were already too dense (with short fibers). As a result, scaffolds after t=30 minutes, were less suitable for future cellular behaviour studies. Consequently, the focus was placed on time points before t=30 minutes.

To better track fiber characteristics, the time intervals were broken down as follow, t=0, t=15, t=20 and t=25. Figure 4.3 shows RCM images of the four conditions. Clear collagen fibers were seen in all conditions (t=0, t=15, t=20 and t=25 minutes). Figure 4.3e-g shows analysis of collagen fibers. Fibers at t=0 (average fiber diameter ~ 2.84 µm, average fiber length ~ 31.67 µm) and t=15 (average fiber diameter ~ 2.72 µm, average fiber length ~ 33.23 µm) were thicker and shorter compared to t=20 (average fiber diameter ~ 2.00 µm, average fiber length ~ 46.14 µm) and t=25 (average fiber

diameter ~ 1.91 µm, average fiber length ~ 44.60 µm). While it was demonstrated that scaffolds at t=20 (average pore size ~ 21.88 μm^2) and t=25 (average pore size ~ 22.88 μm^2) were denser compared to scaffolds at t=0 (average pore size ~ 115.08 μm^2) and t=15 (average pore size ~ 67.96 μm^2).

Together, the results show that the longer we waited to add Fn, the denser scaffolds became with smaller fiber dimeter and longer fiber length. It was observed that scaffolds' microstructure wasn't significantly different when Fn was added at t=20 min and t=25 min. While adding Fn at t=0 min and t=20 min regulate scaffolds' microstructure in terms of fiber diameter, fiber length and density.

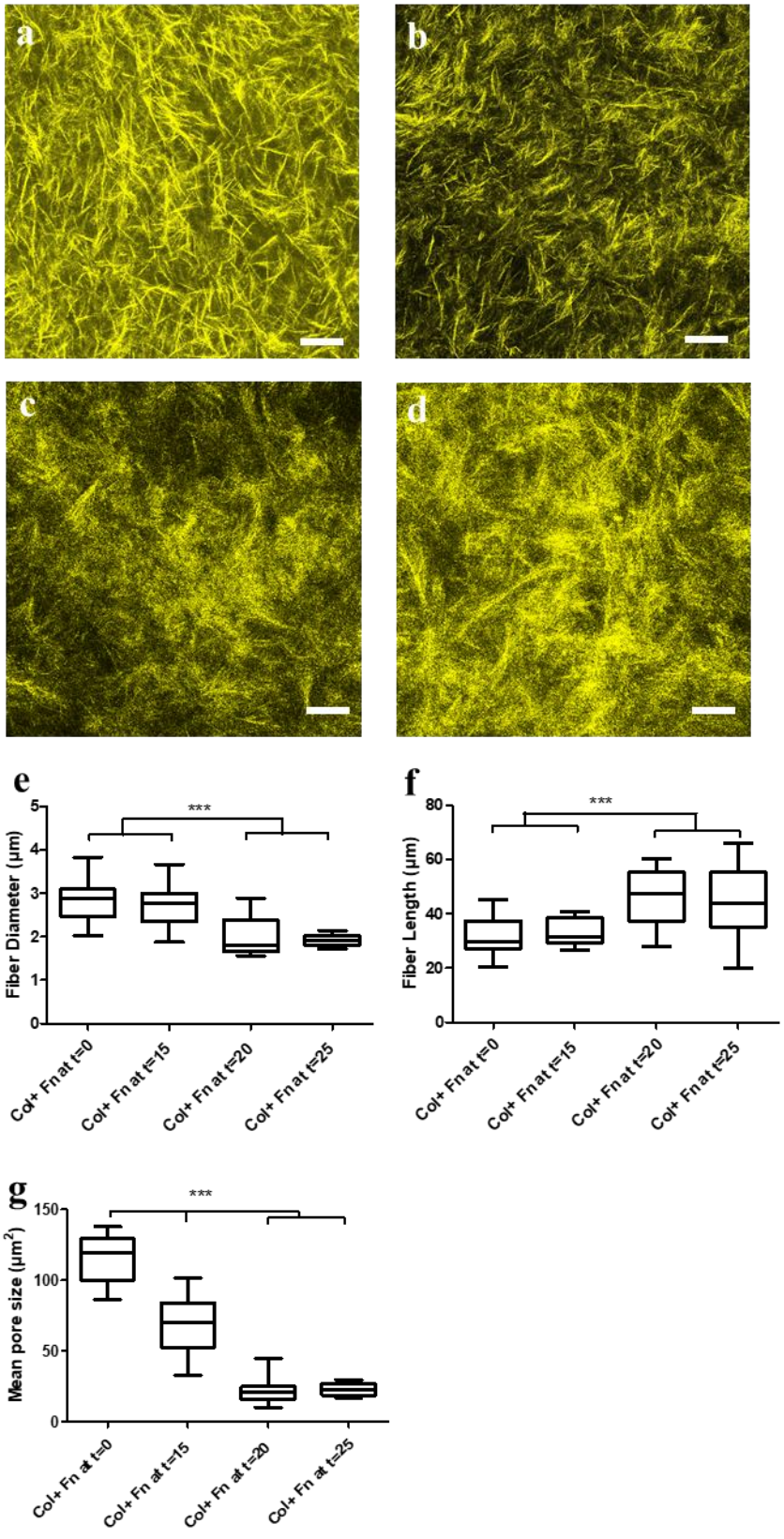
a
b
c
d
e
Fiber Diameter (µm)
***
Col+ Fn at t=0
Col+ Fn at t=15
Col+ Fn at t=20
Col+ Fn at t=25
f
Fiber Length (µm)
***
Col+ Fn at t=0
Col+ Fn at t=15
Col+ Fn at t=20
Col+ Fn at t=25
g
Mean pore size (µm²)
***
Col+ Fn at t=0
Col+ Fn at t=15
Col+ Fn at t=20
Col+ Fn at t=25

Figure 4.3 **Effect of time on the microstructure of 3D cold-cast collagen-Fn scaffolds**. RCM images of collagen scaffolds fabricated at the concentration of 2.88 mg/ml and Fn was added to wells at time (a) t=0 (n=3), averaging around 150 points measurements per sample, (b) t=15 RT-t0 (n=4), averaging around 120 points measurements per sample, (c) t=20 RT-t5 (n=3), averaging around 260 points measurements per sample, (d) t=25 RT-t10 (n=3), averaging around 180 points measurements per sample. Images were analyzed in terms of fiber diameter, mean pore size and fiber length using Fiji. (e) Average fiber diameter of collagen fibers when Fn was added at t=0 (~ 2.84μm), t=15 (~ 2.72μm), t=20 (~ 2.00μm) and t=25 (~ 1.91μm) (f) average fiber length collagen fibers when Fn was added at t=0 (31.67μm), t=15 (~ 33.23μm), t=20 (~ 46.14μm) and t=25 (~ 44.60μm) (g) average mean pore size of collagen fibers when Fn was added at t=0 (~ 115.08μm^2), t=15 (~ 67.96μm^2), t=20 (~ 21.88μm^2) and t=25 (~ 22.88μm^2). Groups are significantly different (***P < 0.0001). Mean ± SD. Scale bars = 50 μm.

4.3.4 Tuning Fibronectin Conformation in Fibrillar Collagen-Fibronectin Scaffolds

We further studied whether Fn conformation could be tuned in our Fn - Col I scaffolds. To monitor Fn conformation during our trials, 10% FRET-labelled Fn was added to Fn solutions. Scaffolds were made as previously described focusing on the two time points of 20 and 25 minutes where clear Fn fibers could be observed. FRET Fn added to collagen scaffolds at t=20 (Figure 4.4a) and t=25 mins (Figure 4.4b). Images were analyzed pixel by pixel with a customized Matlab code to measure FRET ratios (IA/ ID) (Figure 4.4c-d). The analysis showed that Fn fibers were more unfolded (with lower FRET ratios) when FRET Fn was added at t=20 to the scaffolds while when added at t=25 Fn fibers were more compact (with higher FRET ratios) (Figure 4.4e). The results indicate that we have reached a high level of control as not only were collagen fibers tuned in 3D fibrillar Col I - Fn but also conformation of Fn was tracked and tuned. We successfully presented 3D fibrillar dual-protein (collagen and Fn) platforms. Next, cell behaviour in these scaffolds was investigated.

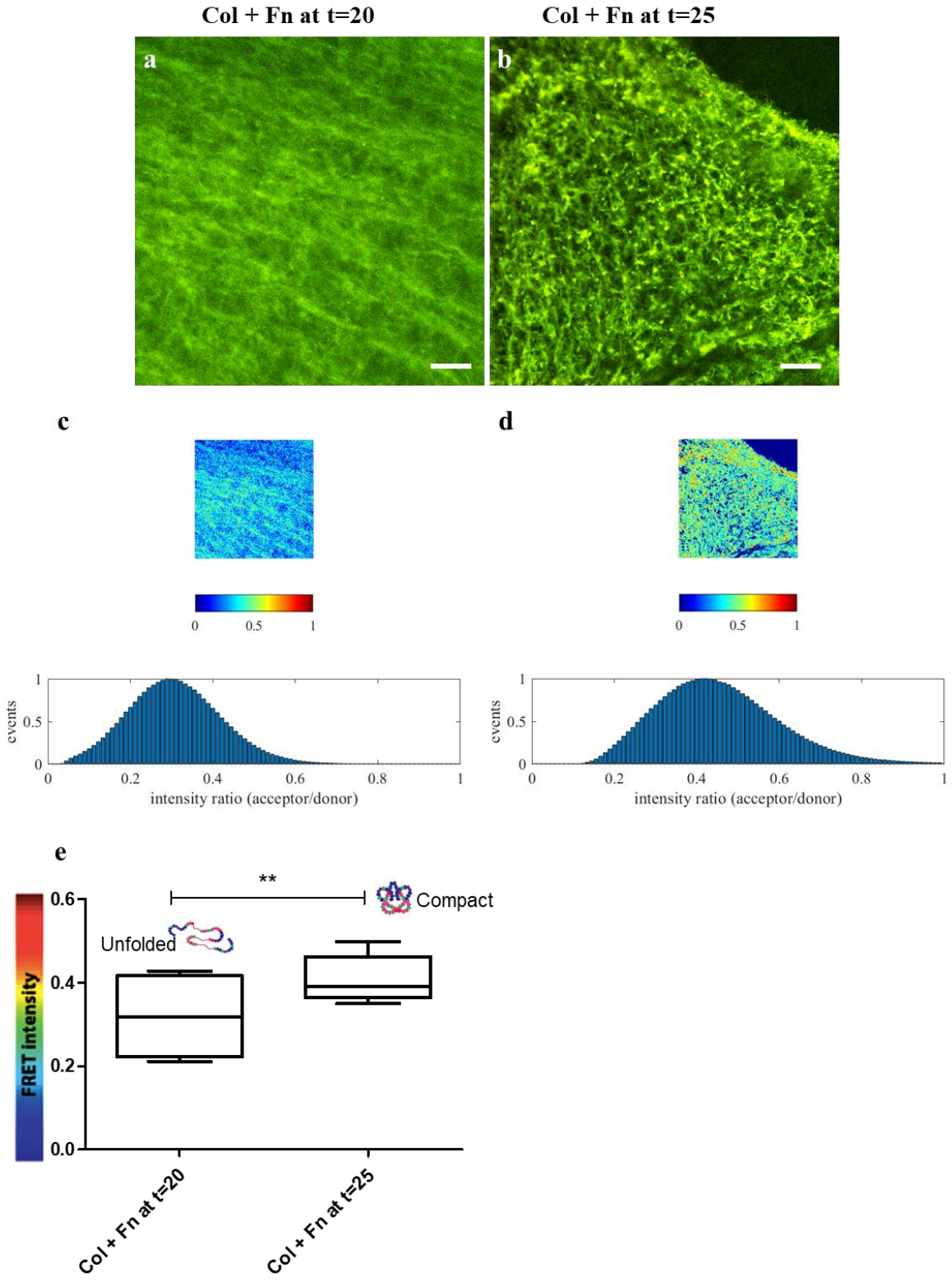
Col + Fn at t=20
Col + Fn at t=25
a
b
c
d
0
0.5
1
events
0.2
0.4
0.6
0.8
intensity ratio (acceptor/donor)
e
**
Compact
Unfolded
FRET intensity
0.6
0.4
0.2
0.0
Col + Fn at t=20
Col + Fn at t=25

Figure 4.4 **Tuning Fn conformation in fibrillar collagen-fibronectin scaffolds**. Fn at solution concentration of 0.2 vol% of which 10% was FRET Fn was added to wells following the incubation of the scaffold in the fridge for 15 mins and then at RT for 5 mins (t20) (a) (n=5) averaging around 140 measurements per sample and for 10 mins (t25) (b) (n=2) averaging around 20 measurements per sample. FRET Fn was double labeled using AlexaFluor 488 and AlexaFluor 546. (c,d) Images were analyzed pixel by pixel with an in-house Matlab code to measure FRET ratio (IA/ ID). The data shows that mean FRET ratio intensity was higher when Fn was added at t=25 which indicating close-to-compact Fn fibers compared to when Fn was added at t=20 where it showed lower FRET intensity ratio unfolded Fn fibers. The two groups are significantly different (**P<0.001, Student's t-test). Mean ± SD. Bar=50 μm.

4.3.5 Cell Behaviour in the Collagen – Fibronectin Scaffolds

Cells interact with their environment by adhering, migrating, remodelling and secreting their own matrix in particular by depositing collagen and fibronectin[7]. Incorporating cells initially in our scaffolds (namely prior to gelation) affects the whole polymerisation dynamics and the resulting structures[15]. Hence, we fabricated cell-embedded scaffolds and went back to investigate a larger range of time points for addition of Fn to the Col I scaffolds including t=0, t=15, t=20, t=25, t=30, t=35 and t=45 minutes. Only the resulting scaffolds with high cohesiveness were chosen to study cell behaviour. Cell adhesion and proliferation on Col I - Fn scaffolds were investigated under three conditions, Fn addition at t=0, t=15 and t=30 min. GFP-3T3 fibroblasts were embedded inside the scaffolds prior to gelation. Scaffolds were fabricated as previously mentioned. Figure 4.5 shows RCM images of the scaffolds combined with fluorescence of GFP-labeled cells. Cells were observed well spread and attached to the scaffold fibers indicating strong cell - matrix interactions and high biocompatibility of the scaffolds. Also, collagen fibers were seen to bundled (Figure 4.5d,f).

Multi-stack images were taken from several fields of view. To calculate cell number, images were analyzed per stack up to 200 μm in thickness for all images. Results were calculated and reported in mm^3 (Figure 4.5). The number of cells in collagen scaffolds incubated for 24h were found to be similar at t=0 (~470 cell/mm^3) and t=30 (~520 cell/mm^3) although lower in scaffolds when Fn was added at t=20 mins (~221 cell/mm^3). A similar trend of cell numbers was observed for 72h culture with the highest number of cells at t=0. Comparing 24h and 72h culture scaffolds, it was noticed that most cells were viable at times up to 72h, some of them giving signs of aggregation at t= 72h

(increased cell-cell interaction). Our data also suggests proliferation in particular at t=0 and t=20 scaffolds where our trend indicates higher number of cells in 72h culture scaffolds. This trend is not visible in the t=30 min sample, likely because of morphological issues with the scaffold itself. Further proof of proliferation is needed. The viability of fibroblasts was investigated using Live /Dead assay. Results suggested that most cells were viable inside the scaffolds after 24h and 72h culture (data not shown).

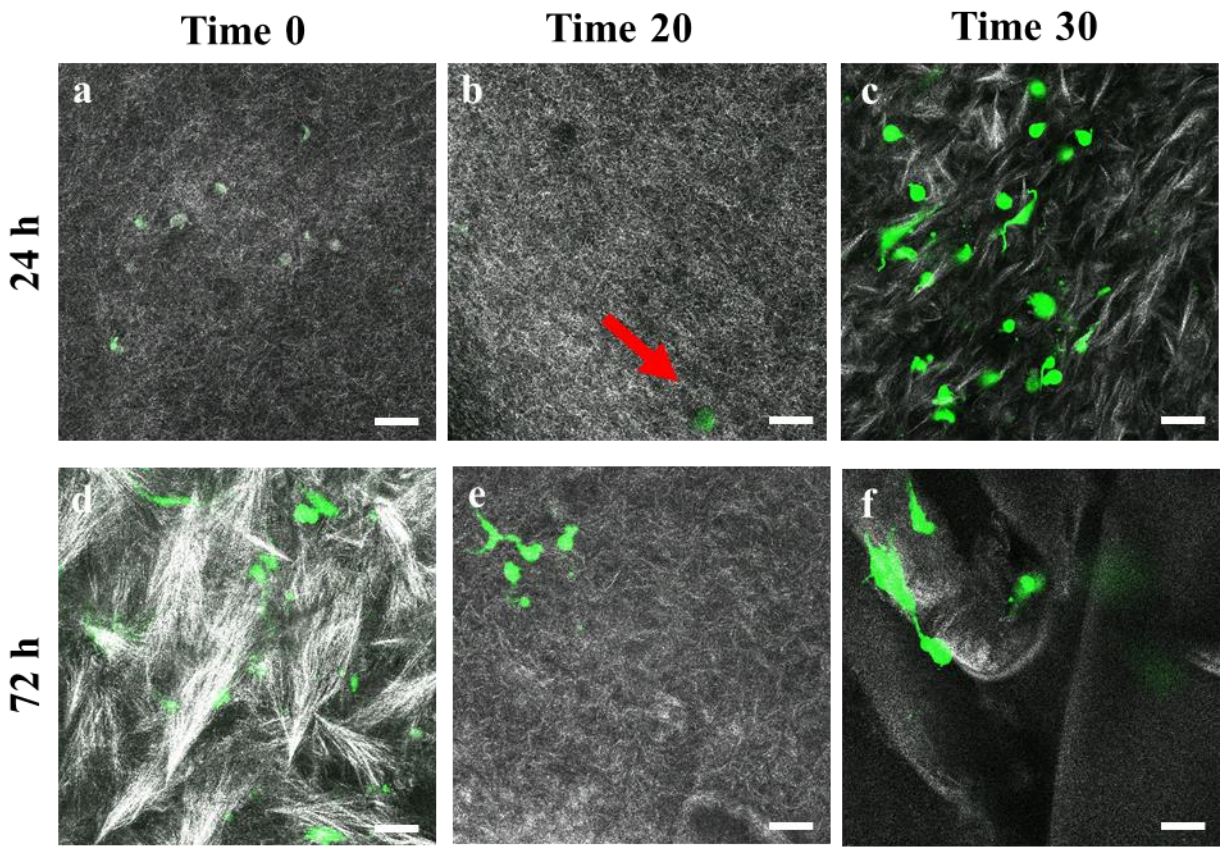
Time 0
Time 20
Time 30
24 h
72 h
a
b
c
d
e
f

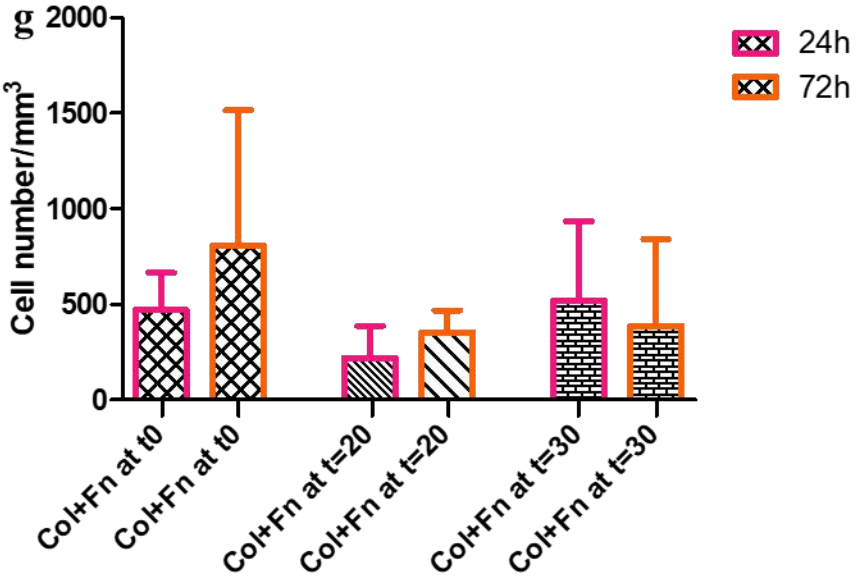
Cell number/mm3
2000
1500
1000
500
0
24h
72h
Col+Fn at t0
Col+Fn at t0
Col+Fn at t=20
Col+Fn at t=20
Col+Fn at t=30
Col+Fn at t=30

Figure 4.5 **Cell-embedded in collagen-Fn scaffolds**. 100k GFP labeled 3T3 cells were added to the collagen solutions at t=0. Fn was added at (a) t=0 (n=6) (b) t=20 (n=5) (the arrow is pointing to the embedded cell) (c) t=30 (n=5) and samples cultured 24h. For a long-term culture of (72 h) Fn was added at (d) t=0 (n=5) (e) t=20 (n=5) (f) t=30 (n=5). (g) Number of cells in short-term (24h) and long-term (72h) culture scaffolds. The average number of cells in 24h at t=0 was (~ 470), t=20 (~ 221) and t=30 (~ 520) and 72h at t=0 (~ 807), t=20 (~ 354) and t=30 (~ 387) were calculated. The data show that cells were viable and proliferated after 24 h in two conditions (t=0 and t=20). Scale bars = 50 μm.

Figure 4.6 shows analysis of collagen fibers. Results demonstrate that short-term cultured scaffolds were significantly different in terms of fiber diameter, length and density. When Fn was added at t=0 and t=20, scaffolds were denser with average pore sizes of around 57.68 and 32.94 μm^2 respectively compared to scaffolds at t=30 with average pore size of around 1176.56 μm^2. Yet, fibers at t=30 were longer (average fiber length ~ 37.44 μm) than fibers at t=0 (average fiber length ~ 15.55 μm) and t=20 (average fiber length ~ 9.29 μm). On the other hand, for long term culture, 72h, fiber diameter was observed to be significantly greater at t=0 compared to t=30, yet similar to t=20, which might be due to fiber bundling. Figure 4.5f suggests that collagen fibers bundled together and created a sheet-like membrane. The fiber length was also greater at t=0 compared to t=20 and t=30. The pore sizes were also significantly bigger at t=0 compared to t=20 and t=30, this is in line with the fiber diameter and length as having longer and thicker fibers could result in larger pores.

Comparing 24h and 72h culture scaffolds, collagen fibers in 72h started to bundle with long fibers resulting in bigger pore sizes while, in 24h scaffolds, no sign of bundling was observed. It is not clear why there is a significant difference between 24h and 72h scaffolds microstructures but it could be attributed to variations in cell interactions and fiber remodelling by embedded cells (further experiments could shed light on this observation).

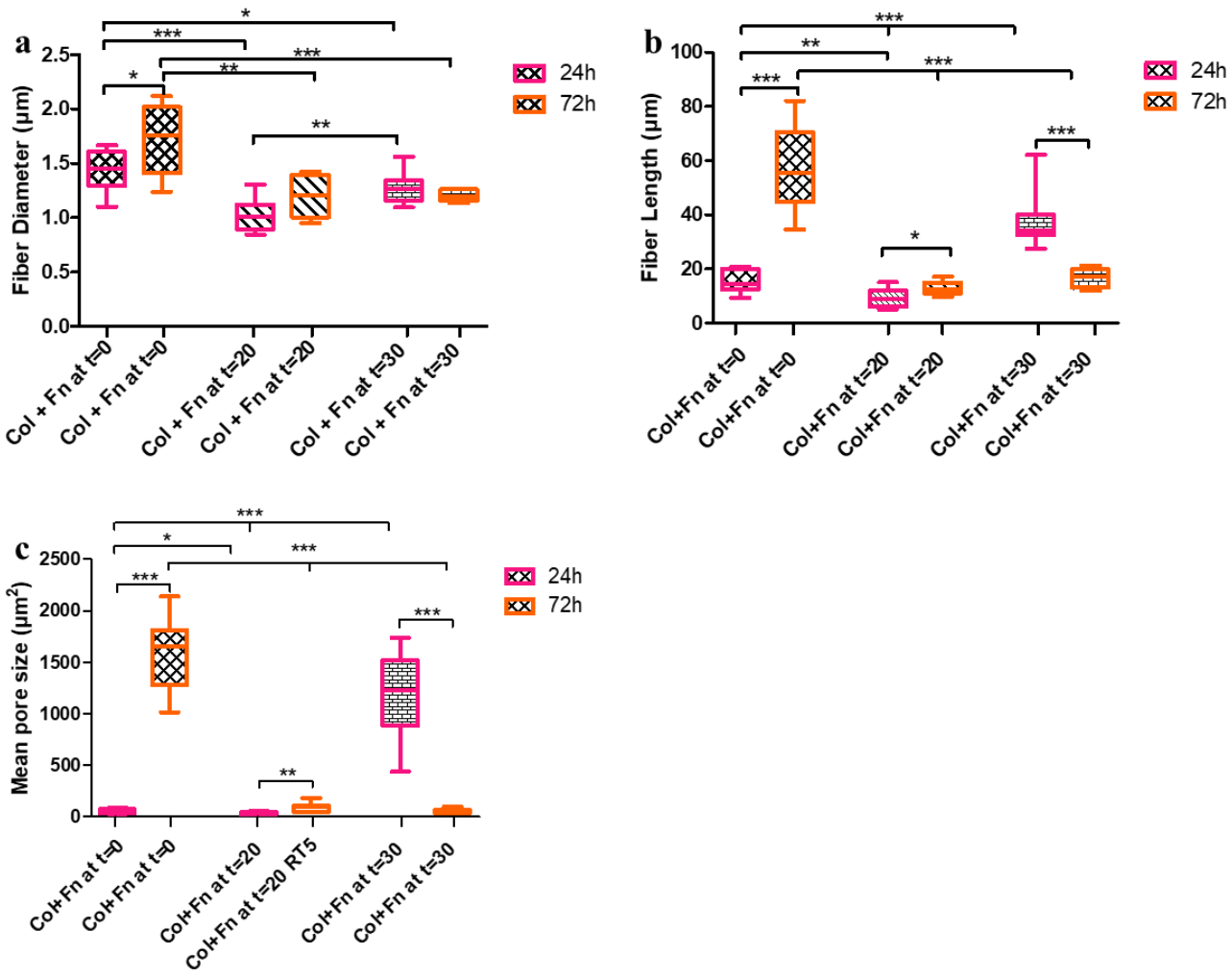

Figure 4.6 **Analysis of the effect of time on the microstructure of cell-embedded in collagen-Fn scaffolds.** Collagen-Fn scaffolds were fabricated at the concentration of 2.88 mg/ml. Fn was added to wells at different time points 0, 20 and 30. RCM images were analyzed in terms of fiber diameter, mean pore size and fiber length using Fiji. (a) Average fiber diameter of collagen fibers when Fn was added at t=0 (n=2), averaging around 150 points measurements per sample, (~ 1.44µm), t=20 (n=2), averaging around 150 points measurements per sample, (~ 1.02µm) and t=30 (n=3), averaging around 230 points measurements per sample, (~ 1.27µm) for 24h and t=0 (n=2), averaging around 180 points measurements per sample, (~ 1.72 µm), t=20 (n=2), averaging around 150 points measurements per sample, (~ 1.20 µm) and t=30 (n=2), averaging around 150 points measurements per sample, (~ 1.20µm) for 72h culture scaffolds. (b) Average mean pore size of collagen fibers when Fn was added at t=0 (~ 57.68 µm^2), t=20 (~ 32.95 µm^2) and t=30 (~ 1176.56 µm^2) for 24h and t=0 (~ 1573.83 µm^2), t=20 (~ 93.44 µm^2) and t=30 (~ 54.97 µm^2) for 72h culture scaffolds. (c) Average fiber length collagen fibers when Fn was added at t=0 (~ 15.55 µm), t=20 (~ 9.30 µm) and t=30 (~ 37.45 µm) for 24h and at t=0 (~ 56.78 µm), t=20 (~ 12.88 µm) and t=30 (~ 16.80 µm) for 72h culture scaffolds. Groups are significantly different (*P < 0.05), (**P < 0.001), (***P< 0.0001). (Student's t-test). Mean ± SD.

4.4 Conclusions

In this chapter we fabricated 3D collagen scaffolds with different fibrillar microstructures using a thermal gradient technique. We investigated the effect of rate of polymerisation and temperature on scaffolds microarchitecture. Our results indicate that, when decreasing polymerisation temperature, scaffold pore size area, fiber diameter and fiber length increased. Our data also suggest that lower temperature leads to denser and stiffer scaffolds.

To better mimic the ECM, we also combined Fn to collagen and studied whether we could control the formation of Fn fibers within the existing collagen scaffolds and create dual proteins fibrillar scaffolds. We investigated the effect of mixing time of Fn within the collagen suspension to control Fn fiber formation. Our results show that Fn fibers could form inside collagen scaffolds when Fn was added at t=20 and 25 minutes. We further monitored the molecular conformation of the formed Fn fibers using FRET-labelled Fn. Our FRET ratio results suggest that Fn fiber conformations could be tuned from compact/relaxed Fn fibers to unfolded/stretched Fn fibers by playing with mixing time. We claim that, to the best of our knowledge, we are the first group to reach such high level of control over dual network structural and conformational properties since both collagen fiber formation and Fn fiber conformation can be tuned independently within our 3D fibrillar Col I - Fn scaffolds.

Additionally, our approach also allowed us to directly encapsulate cells within Col I - Fn scaffolds of various microarchitecture rather than seeding them on top and rely on cell invasion. Our data indicate that cells were viable and well-spread after 72 hr, well distributed and successfully attached to the scaffolds' fibers. Successful cell proliferation was also noted in two scaffolds (when Fn was added at t=0 and t=20) and signs of initial remodelling were observed.

Collectively, our findings indicate that we achieved the fabrication of highly tunable 3D Col I - Fn fibrillar scaffolds with pre-embedded cells, using a combination of temperature-mediated protocols. Such method allowed us to control independently collagen network microarchitecture and Fn conformations. In this framework such scaffolds potentially offer excellent ECM mimicking substrates to monitor cell behaviours in scaffolds with different micro-architectures in large volumes and over long cell culture times.

Chapter 5: General Discussion, Conclusions and Future Directions

5.1 General Discussion

3D Porous Scaffolds

The ECM regulates cell behaviour and signalling in a three dimensional environment[7,125,138]. It contains several macromolecules and proteins among which collagen, which is the most abundant protein providing structural support for cells[17] and fibronectin, which is a crucial mechanotransducer protein ensuring cell adhesion and growth[139]. Studying cell-cell and cell-ECM interactions may pave the way toward the understanding of several complex biological events such as wound healing process and cancer progression. To meet the need for ECM-mimicking structures for long-term cell cultures over large volumes, we proposed two distinct designs and methods for engineering three-dimensional scaffolds mimetics: porous scaffolds made of bulk collagen coated with a fibronectin layer and fibrillar scaffolds made of interconnected collagen and fibronectin fibers.

Freeze-casting is a relatively cheap and easy way of producing porous scaffolds with controlled pore sizes for different types of materials such as ceramics[140], polymers[141], collagen[87] and gelatin[142]. The compressive modulus of the 1.25 wt.% collagen scaffolds used in our study was 1720 ± 300 Pa indicating a good stiffness match with a variety of tissues *in vivo*[143]. Although they were chemically cross-linked to retain cohesiveness and long-term stability in aqueous environments, the biocompatibility of these porous scaffolds was demonstrated, as large populations of cells could successfully invade the structures due to the presence of large interconnected pores that facilitated their migration and communication. The addition of an Fn coating on these collagen scaffolds indicated increased cell adhesion and survival[39]. We thermally controlled the conformation of Fn in the coatings, which allowed us to obtain two categories of Fn-coated scaffolds with controlled protein conformation: compact Fn scaffolds (low temperature deposition) and unfolded Fn scaffolds (high temperature deposition). Our observations are in agreement with previous results obtained on 2D Fn-coated coverglass 8-well chambers in our group where Fn conformation versus temperature followed the same trend. Seeding of fibroblast cells on Fn-coated scaffolds indicated high cell counts on low-temperature coated scaffolds with compact

Fn. These data suggest that cells prefer to interact with the compact Fn scaffolds likely because they can use their most common integrins type, $\alpha_5\beta_1$, while they have to rely on less common (and less numerous) $\alpha_V\beta_3$ integrins to bind to unfolded Fn scaffolds, due to their inability to engage simultaneously the RGD loop and the synergy site of Fn when Fn is unfolded[121,122,144,123].

The ability of cells to perform regular cell functions such as matrix deposition on Fn-coated scaffolds was also investigated. Our findings indicate that not only were cells able to deposit their own matrix in the scaffolds, but also that the conformation of the deposited matrix was significantly different on compact Fn and unfolded Fn coated scaffolds, which demonstrates the high level of control over ECM properties we could reach at early stages (24 hr).

Although an important step was achieved with the fabrication of the above-mentioned scaffolds in terms of control of mechanical and conformational properties (through collagen concentration and temperature of Fn incubation, respectively), both the use of chemical crosslinks that would prevent cell digestion and remodelling and the lack of a genuine fibrillar structure that would better mimetic the physiological ECM led us to change our design and use a different approach.

3D Fibrillar Scaffolds

ECM structural and mechanical properties have a direct effect on promoting diseases. Collagen I regulate both overall structure and mechanics of the bulk ECM and hence various cell signalling functions[9]. In tumor microenvironments, there are bundles of collagen fibers that allow cells to migrate[90]. The aim of our second approach was to engineer scaffolds with genuine fibrillar structures and varied mechanical properties to understand cancer mechanosignalling, in particular tumour growth and metastasis. There are a lot of biological events happening simultaneously in tumour tissues such as cell-tissue interactions, protein remodelling, protein deposition and cell signalling. To get an insight into these biological processes, control over structural and mechanical properties of the microenvironment is required. Cell signalling in tumour microenvironments is different from healthy microenvironments[145]. Cells in tumour microenvironments migrate through bundles of collagen fibers with higher pore size area while in healthy microenvironments, cells migrate through small pores[146,92]. Cell adhesion in 3D environment is more complex than 2D substrates. It is shown that cell adhesion in 3D environment is controlled locally with a direct effect

of matrix rigidity and of number/density of binding sites along matrix fibers. Stiffer environment with bundled collagen fibers, promote single cell adhesion while more compliant networks improve adhesion retraction[146]. *In vitro* during collagen matrix self-assembly, fibrillar architecture is sensitive to various parameters pH, polymerisation temperature, concentration of collagen (available ligand density), which presents the opportunity to tune gels to mimic normal and tumour tissue[147,92].

Several imaging approaches are available to visualize collagen networks at different length scales, including electron microscopy, second harmonic generation imaging, two photon microscopy[148,149,150]. Reflectance microscopy was used in this study to image collagen fibers, analyze fiber properties (length and diameter), and assess scaffold 'porosity'. This imaging modality has the advantage of being non-invasive and label-free. Nonetheless, the penetration depth is limited. Hence, long-distance objectives were required to cover the entire depth of our thick scaffolds.

Our data indicate that, by decreasing polymerisation temperature (cold cast), pore area, fiber length and thickness increased, which was consistent with other studies[92,151,152,153,154]. Longer collagen fibers over less dense areas are likely due to the reduction of nucleation sites resulted in fewer interactions of monomers with polymers[92]. Since cold-casted fibrillar scaffolds allowed cells to migrate and let nutrients flow, we focused on those for (i) further tuning their microarchitecture and (ii) adding the fibronectin fibrillar component.

Fibronectin was incorporated into the above-mentioned scaffolds to engineer more realistic ECM-mimicking scaffolds. In addition to using various temperature gradients (as for porous scaffolds), we also considered the time at which we added fibronectin while collagen scaffolds were polymerising. Our results indicate the presence of clear Fn fibers in coexistence with collagen in two conditions, when Fn was added at t=20 and when added at t=25 minutes. One key applications of intramolecular FRET is to detect protein conformational changes, in particular in Fn molecules[45,51]. Combining FRET and confocal microscopy, we monitored Fn conformation and found a significant difference between our two sets of scaffolds with more compact Fn fibers in scaffolds where Fn was introduced at t=25 while more unfolded Fn fibers were visible in the t=20 samples.

When 3T3s were pre-embedded into the fabricated collagen scaffolds to study cell behaviour, results indicated that cells ended up homogeneously distributed within the whole samples and were viable up to 72h of culture. It was also shown that cells were able to proliferate in scaffolds where Fn was mixed with collagen at t=0 and t=20 minutes. Furthermore, cells were well spread and firmly attached to fibers suggesting strong cell-matrix interaction and highly biocompatibility of our 3D dual protein fibrillar scaffolds.

Similar to many researches, this project and approach has limitations. Although we controlled and tuned scaffolds' microstructure, many parameters still need to be investigated (or at least be finely tuned). Also, it has been difficult to control collagen and fibronectin fibrillogenesis independently. Finally, changing the structural parameters (such as pore size, fiber length etc.) also affect mechanical properties of the scaffolds; as such, it is hard to tune one structural parameter and keep the associated mechanical properties constant and vice versa.

5.2 Conclusions

In this work we generated biocompatible tunable three-dimensional ECM-mimicking scaffolds made of collagen and fibronectin that are able to support various crucial cellular functions such as viability, adhesion, migration and matrix deposition.

In the first approach, porous collagen scaffolds were coated with a layer of fibronectin to better mimic the ECM and the conformation of the fibronectin coating was controlled thermally. 3T3 fibroblast cells seeded on top showed successfully invasion of the scaffolds after 24 hr. Observations proved that cells performed regular cell functions such as cell adhesion and matrix deposition. Our results indicate that a larger number of cells adhered to scaffolds coated with Fn in a compact conformation compared to scaffolds coated with unfolded Fn. Additionally, the effect of Fn conformation also had an effect on early matrix deposition, as cells interacting with the compact Fn coating generated a more compact/relaxed matrix than cells in contact with unfolded Fn, which deposited a stretched and unfolded matrix. To conclude, in this method we engineered 3D porous fibronectin-coated collagen scaffolds in which fibronectin conformation could be thermally switched from compact to unfolded conformation, which in turn regulated fibroblasts adhesion and matrix deposition. Such scaffolds will potentially provide an ECM-mimicking

substrate for cells that can control and monitor cell functions. In order to use porous scaffolds in the context of wound healing, further investigations of cell behaviour in scaffolds including migration assay and quantification of growth factors such as TGF, FGF and VGEF would be required.

In the second approach, fibrillar collagen scaffolds were engineered using temperature-mediated technique. The effect of both polymerisation temperature and collagen concentration was investigated on the scaffolds' microstructure. Our data indicate that, at constant collagen concentration, increasing polymerisation temperature led to decreased pore area, fiber diameter, and fiber length resulting in denser scaffolds. Furthermore, when incorporating Fn into the scaffolds to better recapitulate ECM composition and structure, we investigated both temperature (as in porous scaffolds) and duration of Fn incubation with collagen mixture during polymerisation. Our findings show that we not only got scaffolds in which long and thin Fn fibers were clearly coexisting with the collagen network, but we could also tune the molecular conformation of Fn fibers within the scaffold. Finally, 3T3 fibroblast cells were successfully encapsulated in those scaffolds and remained viable for up to 3 days, indicating strong cell-matrix interactions and high biocompatibility.

In conclusion, in this method we engineered 3D collagen-fibronectin fibrillar scaffolds, which composition and morphology quite accurately recapitulate the cell-deposited ECM. The additional level of control we achieved over molecular conformation within Fn fibers makes these platforms of potential use in cancer research, as they can easily be switched from a compact/relaxed state to an unfolded state, as reported in physiological and pathological conditions, respectively[8].

5.3 Future Directions

Although numerous cell experiments have been performed to prove the biocompatibility of our scaffolds (such as invasion, adhesion, viability, matrix deposition etc), the focus of this thesis work was the design, engineering and characterization of novel 3D ECM-mimicking biomaterials for long term cell cultures over large volumes. More specifically, emphasis was put on investigating and controlling various experimental parameters for scaffolds fabrication, followed by measurements of their composition, structure and conformational to reach optimization.

Future studies will focus on our more physiologically relevant fibrillar scaffolds. Two important aspects are still missing: (i) the characterization of their mechanical properties of scaffolds and (ii) the investigation of more complex and long-term cellular functions in the context of cancer.

In terms of biomechanical properties, the elastic modulus of fibrillar scaffolds needs to be studied to investigate whether the stiffness of scaffolds is in the same range as *in vivo* tissues (and if yes, which tissues?). It is shown that tumor microenvironment is stiffer than healthy tissues[155]. The elastic modulus of controlled Fn-collagen scaffolds could be compared, in order to offer fibrillar scaffolds with varied stiffness to recapitulate healthy and tumor microenvironment. The elastic modulus of the collagen-Fn scaffolds with no cells, would be measured using Dynamic Mechanical Analysis (DMA) technique to report scaffolds overall stiffness. Moreover, it is proven that cells rearrange their microenvironment locally and change the mechanosiganlling[156,157] resulting in altered local stiffness. Several studies have used atomic force microscopy (AFM), to measure stiffness of healthy and tumour tissues locally[158,159]. Local cell interaction toward cell-embedded collagen-Fn scaffolds could be investigated using AFM. The local stiffness of scaffolds could be reported and compared to *in vivo* experiments. Additionally, scaffolds' relaxation should also be quantified, as it is now known that, at constant stiffness, viscosity variations are able to affect important cell functions such as differentiation.

Cellular functions could be focused on cell types, cell behavior such as cell migration, cell-deposited matrix and important features in cancer progression and metastasis including vascularization and angiogenesis, which will be discussed below.

Several cell types including human cells and cancer-associated fibroblasts (CAFs) could be embedded into scaffolds. Since it has been proven that CAFs change their microenvironment by remodelling and rearranging the fibers[160], embedding CAFs into our scaffolds could broaden our knowledge of how the cells remodel the matrix and migrate through bundle in order to achieve its ultimate goal of metastasis. Live imaging assay would help to track the remodeling and migration. The imaging could be done in several time points of t= 24h, 48h and 72h culture. Also, live imaging assay could used when co-culturing human cells and CAFs to give us an insight of the altered mechanosignalling in the tumourous ECM. Moreover, to study cell migration, VEGF could be added to scaffolds to recapitulate vascularized substrates. Then cell migration through remodelled fibers could be tracked by quantifying collagen alignment using directionality plugin in Fiji.

To investigate if cells would behave normally and if they could be able to deposit their own matrix in proposed scaffolds, FRET technique could be applied to analyze the conformation of Fn. Additionally, secreted collagen and Fn could be labeled and the colocalization investigated to give an insight into collagen-fibronectin synergistically effects, fiber rearrangement, and cancer invasion.

Since cancer progression is mainly due to angiogenesis, the effect of vascularized scaffolds on cell behavior will improve our understanding of cancer progression. Several studies have been focused on tumour microenvironment and fibers conformation. It has been shown that fibronectin fibers are more extended in *in vivo* tumour tissues[161], which leads to excess proangiogenic factors secretion[162]. We were able to control fibronectin conformation in our scaffolds. So, the effect of Fn conformation on proangiogenic capability of cells could be investigated by collecting the medium of scaffolds and measuring the VEGF inside the medium using ELISA.

References

1. Lee, E. Y., Parry, G. & J. Bissell, M. Modulation of secreted proteins of mouse mammary epithelial cells by the collagenous substrata. *J. Cell Biol.* **98,** 146–155 (1984).

2. Chiquet, M. Regulation of extracellular matrix gene expression by mechanical stress. *Matrix Biol.* **18,** 417–426 (1999).

3. Engler, A. J., Sen, S., Sweeney, H. L. & Discher, D. E. Matrix Elasticity Directs Stem Cell Lineage Specification. *Cell* **126,** 677–689 (2006).

4. Ingber, D. E. Mechanical signaling and the cellular response to extracellular matrix in angiogenesis and cardiovascular physiology. *Circ. Res.* **91,** 877–887 (2002).

5. Rozario, T. & DeSimone, D. W. The extracellular matrix in development and morphogenesis: A dynamic view. *Dev. Biol.* **341,** 126–140 (2010).

6. Folkman, J. J. & Moscona, A. Role of cell shape in growth control. *Nature* **273,** 345–349 (1978).

7. Järveläinen, H., Sainio, A., Koulu, M., N. Wight, T. & Penttinen, R. Extracellular matrix molecules: potential targets in pharmacotherapy. *Pharmacol Rev.* **61,** 198–223 (2009).

8. Ricard-Blum, S. The Collagen Family. *Cold Spring Harb. Perspect. Biol.* **3,** 1–19 (2011).

9. Lu, P., Weaver, V. M. & Werb, Z. The extracellular matrix: A dynamic niche in cancer progression. *J. Cell Biol.* **196,** 395–406 (2012).

10. Provenzano, P. P., Inman, D. R., Eliceiri, K. W. & Patricia, J. Matrix density-induced mechanoregulation of breast cell phenotype, signaling, and gene expression through a FAK-ERK linkage. *Oncogene* **28,** 4326–4343 (2010).

11. Kauppila, S., Bode, M. K., Stenbäck, F., Risteli, L. & Risteli, J. Cross-linked telopeptides of type I and III collagens in malignant ovarian tumours in vivo. *Br. J. Cancer* **81,** 654–661 (1999).

12. Huijbers, I. J. *et al.* A role for fibrillar collagen deposition and the collagen internalization receptor endo180 in glioma invasion. *PLoS One* **5,** 1–12 (2010).

13. Bosman, F. T. & Stamenkovic, I. Functional structure and composition of the extracellular matrix. *J. Pathol.* **200,** 423–428 (2003).

14. Rauch, F. & Glorieux, F. H. Osteogenesis imperfecta. *Lancet (London, England)* **363,** 1377–85 (2004).

15. Katsuda, S. *et al.* Collagens in human atherosclerosis. Immunohistochemical analysis using collagen type-specific antibodies. *Arterioscler. Thromb. Vasc. Biol.* **12,** 494–502 (1992).

16. Cukierman, E., Pankov, R., Stevens, D. & Yamada, K. Taking Cell-Matrix Adhesions to the Third Dimensions. *Science.* **294,** (2001).

17. Hendriks, J., Riesle, J. & Blitterswijk, C. A. van. Close dependence of fibroblast proliferation on collagen scaffold matrix stiffness. *J. Tissue Eng. Regen. Med.* **4,** 524–531 (2010).

18. Singh, P., Carraher, C. & Schwarzbauer, J. E. Assembly of Fibronectin Extracellular Matrix ECM: extracellular matrix. *Annu. Rev. Cell Dev. Biol* **26,** 397–419 (2010).

19. Romero-López, M. *et al.* Recapitulating the human tumor microenvironment: Colon tumor-derived extracellular matrix promotes angiogenesis and tumor cell growth. *Biomaterials* **116,** 118–129 (2017).

20. Kalluri, R. Basement membranes: Structure, assembly and role in tumour angiogenesis. *Nat. Rev. Cancer* **3,** 422–433 (2003).

21. Parenteau-Bareil, R., Gauvin, R. & Berthod, F. Collagen-based biomaterials for tissue engineering applications. *Materials (Basel).* **3,** 1863–1887 (2010).

22. Fratzl, P., Gupta, H. S., Paschalis, E. P. & Roschger, P. Structure and mechanical quality of the collagen-mineral nano-composite in bone. *J. Mater. Chem.* **14,** 2115–2123 (2004).

23. Mann, V. *et al.* A COL1A1 Sp1 binding site polymorphism predisposes to osteoporotic fracture by affecting bone density and quality. *J. Clin. Invest.* **107,** 899–907 (2001).

24. Rest, M. van der R. & Garrone, R. Collagen family of proteins. *FASEB* **5,** (1991).

25. Halper, J. *Progress in Heritable Soft Connective Tissue Diseases*. **802,** (2014).

26. Prockop, D. J. & Kivirikko, K. I. COLLAGENS : Molecular Biology , Diseases , and Potentials. (1995).

27. Hulmes, D. J. S. Building collagen molecules, fibrils, and suprafibrillar structures. *J. Struct. Biol.* **137,** 2–10 (2002).

28. Cen, L., Liu, W., Cui, L., Zhang, W. & Cao, Y. Collagen tissue engineering: Development of novel biomaterials and applications. *Pediatr. Res.* **63,** 492–496 (2008).

29. Charriere, G., Bejot, M., Schnitzler, L., Ville, G. & Hartmann, D. J. Reactions to a bovine collagen implant: Clinical and immunologic study in 705 patients. *J. Am. Acad. Dermatol.* **21,** 1203–1208 (1989).

30. Yannas, I. V., Burke, J. F., Orgill, D. P. & Skrabut, E. M. Wound tissue can utilize a polymeric template to synthesize a functional extension of skin. *Science.* **215,** 174–176 (1982).

31. Lauer-Fields, J. L. *et al.* Kinetic analysis of matrix metalloproteinase activity using fluorogenic triple-helical substrates. *Biochemistry* **40,** 5795–5803 (2001).

32. Friess, W. Collagen - Biomaterial for drug delivery. *Eur. J. Pharm. Biopharm.* **45,** 113–136 (1998).

33. Trottier, V., Marceau-Fortier, G., Germain, L., Vincent, C. & Fradette, J. IFATS Collection: Using Human Adipose-Derived Stem/Stromal Cells for the Production of New Skin Substitutes. *Stem Cells* **26,** 2713–2723 (2008).

34. Hörmann. Fibronectin and phagocytosis. *Blut* **51,** 307–314 (1985).

35. Wang, K., Seo, B. R., Fischbach, C. & Gourdon, D. Fibronectin Mechanobiology Regulates Tumorigenesis. *Cell. Mol. Bioeng.* **9,** 1–11 (2016).

36. Smith, M. L. *et al.* Force-induced unfolding of fibronectin in the extracellular matrix of living cells. *PLoS Biol.* **5,** 2243–2254 (2007).

37. Constantine, K. L. *et al.* Refined solution structure and ligand-binding properties of PDC-109 domain b. A collagen-binding type II domain. *J. Mol. Biol.* **223,** 281–298 (1992).

38. Bowditch, R. D. *et al.* Identification of a novel integrin binding site in fibronectin:

Differential utilization by beta 3 integrins. *J. Biol. Chem.* **269,** 10856–10863 (1994).

39. Aota, S. I., Nomizu, M. & Yamada, K. M. The short amino acid sequence Pro-His-Ser-Arg-Asn in human fibronectin enhances cell-adhesive function. *J. Biol. Chem.* **269,** 24756–24761 (1994).

40. Potts, J. & Campbell, I. Structure and function of Fibronectin Modules. *Matrix Biol.* **15,** 313–320 (1996).

41. To, W. S. *et al.* Plasma and cellular fibronectin: distinct and independent functions during tissue repair. *Fibrogenesis Tissue Repair* **4,** 21 (2011).

42. Grinnell, F. Fibronectin and wound healing. *Am. J. Dermatopathol.* **4,** (1982).

43. McDonald, J. A., Kelley, D. G. & Broekelmann, T. J. Role of fibronectin in collagen deposition: Fab' to the gelatin-binding domain of fibronectin inhibits both fibronectin and collagen organization in fibroblast extracellular matrix. *J. Cell Biol.* **92,** 485–492 (1982).

44. Foolen, J. *et al.* Full-length fibronectin drives fibroblast accumulation at the surface of collagen microtissues during cell-induced tissue morphogenesis. *PLoS One* **11,** 1–24 (2016).

45. Förster, T. Transfer Mechanisms of Electronic Excitation Energy. *Rudiut. Res. Suppl* **2,** 326–339 (1960).

46. Lakowicz, J. R. *Principles of Fluorescence Spectroscopy Principles of Fluorescence Spectroscopy*. *Principles of fluorescence spectroscopy, Springer, New York, USA, 3rd edn, 2006.* (Springer, 2006). doi:10.1007/978-0-387-46312-4

47. Bajar, B. T., Wang, E. S., Zhang, S., Lin, M. Z. & Chu, J. A guide to fluorescent protein FRET pairs. *Sensors (Switzerland)* **16,** 1–24 (2016).

48. Periasamy, A. Fluorescence resonance energy transfer microscopy: a mini review. *J. Biomed. Opt.* **6,** 287 (2001).

49. Gordon, G. W., Berry, G., Liang, X. H., Levine, B. & Herman, B. Quantitative fluorescence resonance energy transfer measurements using fluorescence microscopy. *Biophys. J.* **74,** 2702–2713 (1998).

50. Periasamy, a & Day, R. N. Visualizing protein interactions in living cells using digitized

GFP imaging and FRET microscopy. *Methods Cell Biol.* **58,** 293–314 (1999).

51. Kubow, K. E. *et al.* Crosslinking of cell-derived 3D scaffolds up-regulates the stretching and unfolding of new extracellular matrix assembled by reseeded cells. *Integr. Biol.* **1,** 635 (2009).

52. Antia, M., Baneyx, G., Kubow, K. E. & Vogel, V. Fibronectin in aging extracellular matrix fibrils is progressively unfolded by cells and elicits an enhanced rigidity response. *Faraday Discuss.* **139,** 229 (2008).

53. Kubow, K. E. *et al.* fibronectin and collagen I in extracellular matrix. *Nat. Commun.* **6,** 1–11 (2015).

54. Jovin, T. & Arndt-Jovin, D. LUMINESCENCE DIGITAL IMAGING MICROSCOPY. *Biophys. J.* **18,** 271–308 (1989).

55. Mitra, R. D., Silva, C. M. & Youvan, D. C. Fluorescence resonance energy transfer between blue-emitting and red- shifted excitation derivatives of the green fluorescent protein. *Gene* **173,** 13–17 (1996).

56. Heim, R. & Tsien, R. Y. Engineering green fluorescent protein for improved brightness, longer wavelengths and fluorescence resonance energy transfer. *Curr. Biol.* **6,** 178–182 (1996).

57. Mere, L. *et al.* Miniaturized FRET assays and microfluidics: Key components for ultra-high-throughput screening. *Drug Discov. Today* **4,** 363–369 (1999).

58. Mein, C. A. *et al.* Evaluation of Single Nucleotide Polymorphism Typing with Invader on PCR Amplicons and Its Automation Evaluation of Single Nucleotide Polymorphism Typing with Invader on PCR Amplicons and Its Automation. 330–343 (2000). doi:10.1101/gr.10.3.330

59. Mátyus, L. Fluorescence resonance energy transfer measurements on cell surfaces. A spectroscopic tool for determining protein interactions. *J. Photochem. Photobiol. B.* **12,** 323–37 (1992).

60. Scholes, G. D. LONG-RANGE RESONANCE ENERGY TRANSFER IN MOLECULAR

SYSTEMS. *Annu. Rev. Phys. Chem.* **54,** 57–87 (2003).

61. Beljonne, D., Curutchet, C., Scholes, G. D. & Silbey, R. J. Beyond Forster Resonance Energy Transfer in Biological and Nanoscale Systems ¨ rster Resonance Energy Transfer in Biological and Nanoscale Systems. **113,** (2009).

62. Ha, T. Single-molecule fluorescence resonance energy transfer. *Methods* **25,** 78–86 (2001).

63. Ha, T. Single-molecule fluorescence methods for the study of nucleic acids. *Curr. Opin. Struct. Biol.* **11,** 287–292 (2001).

64. Antia, M., Islas, L. D., Boness, D. A., Baneyx, G. & Vogel, V. Single molecule fluorescence studies of surface-adsorbed fibronectin. *Biomaterials* **27,** 679–690 (2006).

65. Repesh, L. Fibronectin Involvement in Granulation Tissue and Wound Healing in Rabbits. **LXV,** (1953).

66. Fang, M., Yuan, J., Peng, C. & Li, Y. Collagen as a double-edged sword in tumor progression. *Tumor Biol.* **35,** 2871–2882 (2014).

67. Chen, X. D., Dusevich, V., Feng, J. Q., Manolagas, S. C. & Jilka, R. L. Extracellular matrix made by bone marrow cells facilitates expansion of marrow-derived mesenchymal progenitor cells and prevents their differentiation into osteoblasts. *J. Bone Miner. Res.* **22,** 1943–1956 (2007).

68. Kulinets, I. *Biomaterials and their applications in medicine*. *Regulatory Affairs for Biomaterials and Medical Devices* (Woodhead Publishing Limited, 2014). doi:10.1533/9780857099204.1

69. Ratner, B. D. & Bryant, S. J. Biomaterials: Where We Have Been and Where We Are Going. *Annu. Rev. Biomed. Eng.* **6,** 41–75 (2004).

70. Langer, R. & Tirrell, D. A. Designing materials for biology and medicine. *Nature* **428,** 487–492 (2004).

71. Zhang, N., Yan, H. & Wen, X. Tissue-engineering approaches for axonal guidance. *Brain Res. Rev.* **49,** 48–64 (2005).

72. ATALA, A. Tissue Engineering of Artificial Organs. *J. Endourol.* **14,** 49–57 (2000).

73. Bhattarai, S. R. *et al.* Novel biodegradable electrospun membrane: Scaffold for tissue engineering. *Biomaterials* **25,** 2595–2602 (2004).

74. Reckers, L. J. *et al.* The Role of Fibrin Glue and Suture on the Fixation of Ultra Frozen Preserved Meniscus Transplantation in Rabbits. *Rev. Bras. Ortop. (English Ed.* **44,** 397–403 (2009).

75. Zhang, Y. S. & Khademhosseini, A. Advances in engineering hydrogels. *Science.* **356,** (2017).

76. Madeleine Djabourov, J. L. and P. P. L. Gelation of aqueous gelatin solutions. I. Structural investigation Madeleine. *J. Phys.* **49,** 319–332 (1988).

77. Scholl, F. G., Boucek, M. M., Chan, K. C., Valdes-Cruz, L. & Perryman, R. Preliminary Experience With Cardiac Reconstruction Using Decellularized Porcine Extracellular Matrix Scaffold: Human Applications in Congenital Heart Disease. *World J. Pediatr. Congenit. Hear. Surg.* **1,** 132–136 (2010).

78. Gong, Y. Y. *et al.* A sandwich model for engineering cartilage with acellular cartilage sheets and chondrocytes. *Biomaterials* **32,** 2265–2273 (2011).

79. Cheng, C. W., Solorio, L. D. & Alsberg, E. Decellularized tissue and cell-derived extracellular matrices as scaffolds for orthopaedic tissue engineering. *Biotechnol. Adv.* **32,** 462–484 (2014).

80. Zitnay, J. L. *et al.* Fabrication of dense anisotropic collagen scaffolds using biaxial compression. *Acta Biomater.* **65,** 76–87 (2018).

81. Lu, T., Li, Y. & Chen, T. Techniques for fabrication and construction of three-dimensional scaffolds for tissue engineering. *Int. J. Nanomedicine* **8,** 337–350 (2013).

82. Sultana, N. & Wang, M. PHBV/PLLA-based composite scaffolds fabricated using an emulsion freezing/freeze-drying technique for bone tissue engineering: Surface modification and in vitro biological evaluation. *Biofabrication* **4,** (2012).

83. Schoof, H., Apel, J., Heschel, I. & Rau, G. Control of pore structure and size in freeze-dried collagen sponges. *J. Biomed. Mater. Res.* **58,** 352–357 (2001).

84. Zhang, S. Fabrication of novel biomaterials through molecular self-assembly. *Nat. Biotechnol.* **21,** 1171–1178 (2003).

85. Piez, K. A. History of extracellular matrix: A personal view. *Matrix Biol.* **16,** 85–92 (1997).

86. Long, Y. *et al.* Collagen−hydroxypropyl methylcellulose membranes for corneal regeneration. *ACS Omega* **3,** 1269–1275 (2018).

87. Wan, A. M. D. *et al.* 3D conducting polymer platforms for electrical control of protein conformation and cellular functions. *J. Mater. Chem. B* **3,** 5040–5048 (2015).

88. Lou, J., Stowers, R., Nam, S., Xia, Y. & Chaudhuri, O. Stress relaxing hyaluronic acid-collagen hydrogels promote cell spreading, fiber remodeling, and focal adhesion formation in 3D cell culture. *Biomaterials* **154,** 213–222 (2018).

89. Gillette, B. M. *et al.* Engineering extracellular matrix structure in 3D multiphase tissues. *Biomaterials* **32,** 8067–8076 (2011).

90. Conklin, M. W. *et al.* Aligned collagen is a prognostic signature for survival in human breast carcinoma. *Am. J. Pathol.* **178,** 1221–1232 (2011).

91. McCoy, M. *et al.* Collagen Fiber Orientation regulates 3D Vascular Network Formation and Alignment. *ACS Biomater. Sci. Eng.* acsbiomaterials.8b00384 (2018). doi:10.1021/acsbiomaterials.8b00384

92. Staunton, J. R. *et al.* Mechanical properties of the tumor stromal microenvironment probed in vitro and ex vivo by in situ-calibrated optical trap- based active microrheology. *Cell. Mol. Bioeng.* **18,** 386–392 (2015).

93. Chen, X. *et al.* Peptide-Modified Chitosan Hydrogels Accelerate Skin Wound Healing by Promoting Fibroblast Proliferation, Migration, and Secretion. *Cell Transplant.* **26,** 1331–1340 (2017).

94. Robson, M. C. Wound healing: biologic features and approaches to maximum healing trajectories. *Curr. Probl. Surg.* **38,** 72–141 (2001).

95. Medrado, A. R. A. P., Pugliese, L. S., Reis, S. R. A. & Andrade, Z. A. Influence of low level laser therapy on wound healing and its biological action upon myofibroblasts. *Lasers Surg.*

Med. **32,** 239–244 (2003).

96. Witte, M. B. & Barbul, A. General Principles of Wound Healing. *Surg. Clin. North Am.* **77,** 509–528 (1997).

97. Clark, R. A. F. Regulation of fibroplasia in cutaneous wound repair. *American Journal of the Medical Sciences* **306,** 42–48 (1993).

98. Yang, L., Witten, T. M. & Pidaparti, R. M. A biomechanical model of wound contraction and scar formation. *J. Theor. Biol.* **332,** 228–248 (2013).

99. Schäfer, M. & Werner, S. Cancer as an overhealing wound: An old hypothesis revisited. *Nat. Rev. Mol. Cell Biol.* **9,** 628–638 (2008).

100. Dolberg, D. S. ., Hollingsworth, R., Hertle, M. & Bissell, M. J. . Wounding and its Role in RSV-Mediated Tumor Formation. *Am. Assoc. Adv. Sci.* **230,** 676–678 (1985).

101. F. Dvorak, H. TOUMORS: WOUNDS THAT DO NOT HEAL. Similarities between Tumor Stroma Generation and Wound Healing. **315,** 1650–1659 (1986).

102. Balkwill, F., Charles, K. A. & Mantovani, A. Smoldering and polarized inflammation in the initiation and promotion of malignant disease. *Cancer Cell* **7,** 211–217 (2005).

103. Jaafar, H., Sharif, S. E. T. & Murtey, M. Das. Pattern of collagen fibers and localization of matrix metalloproteinase 2 and 9 during breast cancer invasion. *Tumori* **100,** e204–e211 (2014).

104. Wang, K. *et al.* Stiffening and unfolding of early deposited-fibronectin increase proangiogenic factor secretion by breast cancer-associated stromal cells. *Biomaterials* **54,** 63–71 (2015).

105. Christensen, L., Nielsen, M., Holund, B. & Clemmensen, I. In vivo demonstration of cytoplasmic fibronectin in human breast carcinomas. *Virchows Arch* **407,** 337–346 (1985).

106. Asch, B. B., Kamat, B. R. & Burstein, N. A. Interactions of Normal, Dysplastic, and Malignant Mammary Epithelial Cells with Fibronectin in Vivo and in Vitro. *Cancer Res.* **41,** 2115–2125 (1981).

107. Provenzano, P. P. *et al.* Collagen reorganization at the tumor-stromal interface facilitates

local invasion. *BMC Med.* **4,** 1–15 (2006).

108. Clark, R. A. F. *et al.* Blood vessel fibronectin increases in conjunction with endothelial cell proliferation and capillary ingrowth during wound healing. *J. Invest. Dermatol.* **79,** 269–276 (1982).

109. Kim, S., Bell, K., Mousa, S. A. & Varner, J. A. Regulation of angiogenesis in vivo by ligation of integrin α5β1 with the central cell-binding domain of fibronectin. *Am. J. Pathol.* **156,** 1345–1362 (2000).

110. Kass, L., T.Erler, J., Dembo, M. & Weaver, V. M. Mammary epithelial cell: Influence of extracellular matrix composition and organization during development and tumorigenesis. *Int. J. Biochem Cell Biol.* **39,** 1987–1994 (2007).

111. Schedin, P. & Keely, P. J. Mammary gland ECM remodeling, stiffness, and mechanosignaling in normal development and tumor progression. *Cold Spring Harb. Perspect. Biol.* **3,** 1–22 (2011).

112. Balcioglu, H. E., van de Water, B. & Danen, E. H. J. Tumor-induced remote ECM network orientation steers angiogenesis. *Sci. Rep.* **6,** 22580 (2016).

113. Kim, T. E. *et al.* Three-dimensional culture and interaction of cancer cells and dendritic cells in an electrospun nano-submicron hybrid fibrous scaffold. *Int. J. Nanomedicine* **11,** 823–835 (2016).

114. Zhang, X., Li, C. & Luo, Y. Aligned/unaligned conducting polymer cryogels with three-dimensional macroporous architectures from ice-segregation-induced self-assembly of PEDOT-PSS. *Langmuir* **27,** 1915–1923 (2011).

115. Davidenko, N. *et al.* Biomimetic collagen scaffolds with anisotropic pore architecture. *Acta Biomater.* **8,** 667–676 (2012).

116. Shahini, A. *et al.* 3D conductive nanocomposite scaffold for bone tissue engineering. *Int. J. Nanomedicine* **9,** 167–181 (2014).

117. Shin, H., Jo, S. & Mikos, A. G. Biomimetic materials for tissue engineering. *Biomaterials* **24,** 4353–4364 (2003).

118. Lungu, A. *et al.* Superporous collagen-sericin scaffolds. *J. Appl. Polym. Sci.* **127,** 2269–2279 (2013).

119. Wang, J. H. C. & Lin, J. S. Cell traction force and measurement methods. *Biomech. Model. Mechanobiol.* **6,** 361–371 (2007).

120. Millan, L. & Marchi, E. Temperature effect on collagen-like structure. *Math. Model.* **8,** 654–658 (1987).

121. García, A. J., Schwarzbauer, J. E. & Boettiger, D. Distinct activation states of α5β1 integrin show differential binding to RGD and synergy domains of fibronectin. *Biochemistry* **41,** 9063–9069 (2002).

122. Danen, E. H. J. *et al.* Requirement for the Synergy Site for Cell Adhesion to Fibronectin Depends on the Activation State of Integrin α 5 β 1. *Biol. Chem.* **270,** 1–8 (1995).

123. Sechler, J. L., Corbett, S. A. & Schwarzbauer, J. E. Modulatory Roles for Integrin Activation and the Synergy Site of Fibronectin during Matrix Assembly. *Mol. Biol. Cell* **8,** 2563–2573 (1997).

124. Yang, Y., Wang, K., Gu, X. & Leong, K. Biophysical Regulation of Cell Behavior—Cross Talk between Substrate Stiffness and Nanotopography. **3,** 36–54 (2017).

125. Humphrey, J. D., Dufresne, E. R. & Schwartz, M. A. Mechanotransduction and extracellular matrix homeostasis. *Nat. Rev. Mol. Cell Biol.* **15,** 802–812 (2014).

126. Hennink, W. E. & van Nostrum, C. F. Novel crosslinking methods to design hydrogels. *Adv. Drug Deliv. Rev.* **64,** 223–236 (2012).

127. Lu, P., Weaver, V. M. & Werb, Z. The extracellular matrix: a dynamic niche in cancer progression. *J. Cell Biol.* **196,** 395–406 (2012).

128. Gattazzo, F., Urciuolo, A. & Bonaldo, P. Extracellular matrix: A dynamic microenvironment for stem cell niche. *Biochim. Biophys. Acta - Gen. Subj.* **1840,** 2506–2519 (2014).

129. Montell, D. J. Morphogenetic Cell Movements : Diversity from Modular Mechanical Properties. *Science.* **322,** 1502–1505 (2008).

130. Lowe, C. J., Reucroft, I. M., Grota, M. C. & Shreiber, D. I. Production of Highly Aligned Collagen Scaffolds by Freeze-drying of Self-assembled, Fibrillar Collagen Gels. *ACS Biomater. Sci. Eng.* **2,** 643–651 (2016).

131. Goyal, R. *et al.* Development of hybrid scaffolds with natural extracellular matrix deposited within synthetic polymeric fibers. *J. Biomed. Mater. Res. - Part A* **105,** 2162–2170 (2017).

132. Malandrino, A., Mak, M., Kamm, R. D. & Moeendarbary, E. Complex mechanics of the heterogeneous extracellular matrix in cancer. *Extrem. Mech. Lett.* **21,** 25–34 (2018).

133. Robertson, C. The extracellular matrix in breast cancer predicts prognosis through composition, splicing, and crosslinking. *Exp. Cell Res.* **343,** 73–81 (2016).

134. Zhang, Y., Xu, B. & Chow, M. J. Experimental and modeling study of collagen scaffolds with the effects of crosslinking and fiber alignment. *Int. J. Biomater.* **2011,** (2011).

135. Birk, D. & Trelstad, R. Fibroblasts Create Compartments in the Extracellular Space Where Collagen Polymerizes into Fibrils and Fibrils Associate into Bundles. *Ann. N. Y. Acad. Sci* 258–266 (1985).

136. Birk, D. E. & Trelstad, R. L. Extracellular compartments in tendon morphogenesis: Collagen fibril, bundle, and macroaggregate formation. *J. Cell Biol.* **103,** 231–240 (1986).

137. Birk, D. E. & Trelstad, R. L. Extracellular compartments in matrix morphogenesis: Collagen fibril, bundle, and lamellar formation by corneal fibroblasts. *J. Cell Biol.* **99,** 2024–2033 (1984).

138. Schwartz, M. A., Schaller, M. D. & Ginsberg, M. H. Integrins: Emerging Paradigms of Signal Transduction. *Annu. Rev. Cell Dev. Biol.* **11,** 549–599 (1995).

139. Hynes, R. *Fibronectins*. (New York : Springer-Verlag, 1990).

140. Deville, S. Freeze-casting of porous ceramics: A review of current achievements and issues. *Adv. Eng. Mater.* **10,** 155–169 (2008).

141. Zhang, H. *et al.* Aligned two- and three-dimensional structures by directional freezing of polymers and nanoparticles. *Nat. Mater.* **4,** 787–793 (2005).

142. Ren, L., Tsuru, K., Hayakawa, S. & Osaka, A. Novel approach to fabricate porous gelatin-

siloxane hybrids for bone tissue engineering. *Biomaterials* **23,** 4765–4773 (2002).

143. Akhtar, R., Sherratt, M. J., Cruickshank, J. K. & Derby, B. Characterizing the elastic properties of tissues. *Mater. Today* **14,** 96–105 (2011).

144. Mould, A. P. *et al.* Defining the topology of integrin a5b1-fibronectin interactions using inhibitory anti-a5 and anti-b1 monoclonal antibodies. *J. Biol. Chem.* **272,** 17283–17292 (1997).

145. Hanahan, D. & Weinberg, R. Hallmarks of cancer: The next generation. *Cell* **144,** 646–674 (2011).

146. Doyle, A. D., Carvajal, N., Jin, A., Matsumoto, K. & Yamada, K. M. Local 3D matrix microenvironment regulates cell migration through spatiotemporal dynamics of contractility-dependent adhesions. *Nat. Commun.* **6,** 1–15 (2015).

147. Raub, C. B. *et al.* Noninvasive Assessment of Collagen Gel Microstructure and Mechanics Using Multiphoton Microscopy. *Biophys. J.* **92,** 2212–2222 (2007).

148. Kadler, K. E., Holmes, D. F., Trotter, J. A. & Chapman, J. A. Collagen fibril formation. *J. Biochem.* **316,** 1–11 (1996).

149. Cox, G. *et al.* 3-Dimensional imaging of collagen using second harmonic generation. *J. Struct. Biol.* **141,** 53–62 (2003).

150. Zoumi, A., Yeh, A. & Tromberg, B. J. Imaging cells and extracellular matrix in vivo by using second-harmonic generation and two-photon excited fluorescence. *Proc. Natl. Acad. Sci. U. S. A.* **99,** 11014–9 (2002).

151. Bredfeldt, J. S. *et al.* Computational segmentation of collagen fibers from second-harmonic generation images of breast cancer. *J. Biomed. Opt.* **19,** 016007 (2014).

152. Tilbury, K. & Campagnola, P. J. Applications of second-harmonic generation imaging microscopy in ovarian and breast cancer. *Perspect. Medicin. Chem.* **7,** 21–32 (2015).

153. Wood, G. C. & Keech, M. K. The formation of fibrils from collagen solutions 1. The effect of experimental conditions: kinetic and electron-microscope studies. *Biochem. J.* **75,** 588–598 (1960).

154. McPherson, J. M. *et al.* Collagen Fibrillogenesis In Vitro: A Characterization of Fibril Quality as a Function of Assembly Conditions. *Top. Catal.* **5,** 119–135 (1985).

155. Paszek, M. J. *et al.* Tensional homeostasis and the malignant phenotype. *Cancer Cell* **8,** 241–254 (2005).

156. Liu, Y. J. *et al.* Differential Transmission of Actin Motion Within Focal Adhesions. *Science.* **315,** 111–115 (2007).

157. Gardel, M. L., Schneider, I. C., Aratyn-Schaus, Y. & Waterman, C. M. Mechanical Integration of Actin and Adhesion Dynamics in Cell Migration. *Annu. Rev. Cell Dev. Biol.* **26,** 315–333 (2010).

158. Plodinec, M. *et al.* The nanomechanical signature of breast cancer. **7,** (2012).

159. Acerbi, I. *et al.* Human breast cancer invasion and aggression correlates with ECM stiffening and immune cell infiltration. *Integr. Biol. (United Kingdom)* **7,** 1120–1134 (2015).

160. Wang, K. *et al.* Breast cancer cells alter the dynamics of stromal fibronectin-collagen interactions. *Matrix Biol.* **60–61,** 86–95 (2017).

161. Chandler, E. M., Saunders, M. P., Yoon, C. J., Gourdon, D. & Fischbach, C. Adipose progenitor cells increase fibronectin matrix strain and unfolding in breast tumors. *Phys. Biol.* **8,** (2011).

162. Wan, A. M. D. *et al.* Fibronectin conformation regulates the proangiogenic capability of tumor-associated adipogenic stromal cells. *Biochim Biophys Acta* **9,** 4314–4320 (2013).